

Decimetric-resolution stochastic inversion of shallow marine seismic reflection data; dedicated strategy and application to a geohazard case study

Giuseppe Provenzano^{*}, Mark E. Vardy[†], Timothy J. Henstock^{*}

SUMMARY

Characterisation of the top 10-50 m of the subseabed is key for landslide hazard assessment, offshore structure engineering design and underground gas-storage monitoring. In this paper, we present a methodology for the stochastic inversion of ultra-high-frequency (UHF, 0.2-4.0 kHz) pre-stack seismic reflection waveforms, designed to obtain a decimetric-resolution remote elastic characterisation of the shallow sediments with minimal pre-processing and little a-priori information. We use a genetic algorithm in which the space of possible solutions is sampled by explicitly decoupling the short and long wavelengths of the P-wave velocity model. This approach, combined with an objective function robust to cycle skipping, outperforms a conventional model parametrisation when the ground-truth is offset from the centre of the search domain. The robust P-wave velocity model is used to precondition the width of the search range of the multi-parameter elastic inversion, thereby improving the efficiency in high dimensional parametrizations. Multiple independent runs provide a set of independent results from which the reproducibility of the solution can be estimated. In a real dataset acquired in Finneidfjord, Norway, we also demonstrate the sensitivity of UHF seismic inversion to shallow subseabed anomalies that play a role in submarine slope stability. Thus, the methodology has the potential to become an important practical tool for marine ground model building in spatially heterogeneous areas, reducing the reliance on expensive and time-consuming coring campaigns for geohazard mitigation in marine areas.

Key words: Inverse theory - Controlled source seismology - Acoustic properties - Geomechanics

1 INTRODUCTION

A quantitative high-resolution physical model of the top 50 m of the seabed is of key importance for a wide range of geohazard and offshore engineering applications: identification of potential shallow landsliding (Vanneste et al., 2013); monitoring of gas storage sites (Cevatoglu et al., 2015); and assessment of offshore structures stability (Vardy et al., 2012). Currently, engineering-scale sediment characterisation relies heavily on direct sampling of the seabed and in-situ measurements (e.g. Stoker et al., 2009). This is expensive and time-consuming for large areas, as well as being liable to alter the sediment properties during the coring process (Clare et al., 2017; Monrigal et al., 2017; M. E. Vardy et al., 2017).

Variations in lithology and pore-pressure conditions produce mechanical layering in the shallow subsurface, that can be conducive to changes in the stability conditions of submarine slopes (Vardy et al., 2012; Vanneste et al., 2013). Corresponding anomalies in compressibility, shear resistance and density, have recognisable footprints on the amplitude and phase of the multi-offset reflected seismic waveforms (Ostrander, 1984; Ruthenford & Williams, 1989). Therefore, seismic reflection data have the potential to be used as a remote sensing tool for shallow geohazard estimation (Mallick & Dutta, 2002; Vardy et al., 2017). As opposed to reservoir-scale seismic exploration, ultra-high-frequency (UHF, 0.2-4.0 kHz) multi-channel marine seismic reflection data are historically under-used in industry for offshore engineering design, being most often limited to a semi-quantitative interpretation of the reflection amplitudes and facies geometries. Recent advances, however, have shown the potential use of UHF data as a quantitative tool (Vardy et al., 2017), from acoustic quality factor estimation (Pinson et al., 2008) and acoustic impedance inversion (Vardy, 2015), to elastic pre-stack inversion of the full waveform (Provenzano et al., 2016, 2017).

* Ocean and Earth Science, National Oceanography Centre Southampton, University of Southampton, European Way, Southampton, SO14 3ZH

† Marine Geosciences Group, National Oceanography Centre, Southampton, European Way, Southampton, SO14 3ZH

Full waveform inversion (FWI) is a process by which the initial state of knowledge about a given parametrisation of the propagation medium (model) is iteratively improved, by maximising the fitness between the observed seismograms and the data computed using a forward modelling operator that approximates the wave equation (Mora, 1980; Tarantola, 1984; Virieux & Operto, 2009). The oscillating nature of the data makes the high-frequencies of the inversion strongly non-linear with respect to the long-wavelengths of the P-wave model (cycle skipping; Tarantola, 1984; Fichtner, 2011), and non-linearity is enhanced by the interdependency among the different elastic parameters (Operto et al., 2013; Gholami et al., 2013a,b). A deterministic inversion thus requires an accurate starting model and an equally accurate estimation of the Hessian matrix (Virieux & Operto, 2009; Fichtner, 2011; Operto et al., 2013; Dagnino et al., 2014).

Alternatively, the inversion can be tackled with a stochastic approach, which samples the model space with a density proportional to the *Posterior Probability Density function (PPD)* (Sambridge & Mosegaard, 2002; Sen & Stoffa, 2013). In addition to being less reliant upon the accuracy of the starting solution, stochastic seismic inversion, in principle, allows lots of potentially useful information on the performance of the inversion to be extracted from the PPD (Sambridge, 1999; Tarantola, 2005). This includes, but it's not limited to, the multi-parameter solution uncertainties and crosstalk resulting from the noise content, the limited offset and bandwidth of the data, and the inherent interdependency of coupled parameters. However, most often deterministic FWI is the only feasible approach in three-dimensional environments because of the high number of model evaluations required in high-dimensionality spaces and the computing cost of the seismogram modelling.

Stochastic optimisers such as Genetic Algorithm (Goldberg, 1989), Simulated Annealing (Rothman, 1985) and Particle Swarm Optimisation (Kennedy & Eberhart, 1995), implement analogies between numerical optimisation and natural biological and physical phenomena. They represent a compromise between the extensive exploration of the model space, and the exploitation of the current state of information about the model (Sambridge & Mosegaard, 2002). Although providing a biased posterior distribution of models (Sambridge & Mosegaard, 2002; Sambridge, 1999; Sen & Stoffa, 1996; Aleardi & Mazzotti, 2017), they are computationally more affordable than a

pure Bayesian approach, and more robust against local minima entrapment than a deterministic algorithm (Tarantola, 1984; Sen & Stoffa, 2013; Sambridge & Mosegaard, 2002).

These algorithms have been applied to FWI of both land and marine data, for reservoir characterisation and shallow drilling hazard assessment, (Stoffa & Sen, 1991; Sen & Stoffa, 1992; Mallick & Dutta, 2002; Mallick & Adhikari, 2015; Sajeve et al., 2016; Aleardi & Mazzotti, 2017), especially when a one-dimensional parametrisation of the problem is sensible, and hence the number of unknowns lower. Stochastic optimisers would be especially beneficial to the inversion of seismic data for shallow geohazard purposes, because of the difficulties of obtaining a reliable starting elastic model from a typical UHF reflection dataset, as well as the capability of providing solution error bounds for geological interpretation and engineering design (Morgan et al., 2014; Vardy, 2015; Vardy et al., 2015).

In this paper we present a sub-metric resolution stochastic seismic inversion methodology based upon a genetic algorithm, custom-built for limited offset, limited bandwidth seismic reflection data. The performance of the stochastic algorithm is tested on both synthetic and real data. In summary, this paper aims at demonstrating that:

- (i) Our proposed strategy is effective at reducing the dependency from the search range design compared to a genetic algorithm with a conventional parametrisation.
- (ii) A two-stage multi-parameter inversion with data-driven preconditioning improves the performance of the inversion, and the interpretability of the estimated elastic model.
- (iii) Elastic layering, corresponding to key-features for slope instability, can be successfully identified and quantitatively described; in an area subject to shallow landsliding (Finneidfjord, northern Norway). A sediment bed corresponding to the glide plane of multiple-landslide events is accurately located and its changes in pore-fluid saturation quantified.

This underpins the application of UHF seismic reflection data as a remote sensing tool for ground-model building and geohazard estimation, reducing the need for expensive and time-consuming coring campaigns.

2 DATA AND METHODOLOGY OUTLINE

2.1 Example estimation of a starting model from UHF data

Shallow marine seismic reflection data typically suffer from the limited offset and lack of low frequencies of the source-acquisition system, which severely limits the sensitivity to the broad-band multi-parameter space (Mora, 1980; Jannane, 1989). Furthermore, most shallow marine datasets are single-component and do not contain post-critical reflections, which limits the possibility of uncoupling the effect of the different elastic parameters (Kormendi & Dietrich, 1991), as well as the sensitivity to the long wavelength distribution of shear properties and density (Operto et al., 2013; Provenzano et al., 2017). As a result, the solution of the inverse problem is highly dependent upon the starting model (Virieux & Operto, 2009; Operto et al., 2013).

In high-resolution reflection seismic data, due to the limited aperture, a starting model is typically obtained from limited-offset normal-move-out velocity analysis (e.g. Aleardi et al., 2016), from which an interval P-wave velocity profile is derived (Dix, 1955). The uncertainty associated with this process can be high, and bias the seismic inversion towards unreliable solutions.

As an example, we simulate a synthetic UHF seismic reflection dataset (Fig. 1a), acquired in a shallow marine context with a one-dimensional isotropic elastic shallow subsurface (Fig. 1b); the model is a 7-m thick stack of 30 homogeneous layers, representing a site with a strong P-wave velocity gradient and properties reasonable for near-surface sediments (Hamilton, 1970). We suppose no data-independent information is available in the site about the P-wave velocity trend, and we want to derive interval velocities from reflection moveout semblance analysis.

The source wavelet is the signature of a Boomer electro-acoustic plate, whose effective bandwidth spans from 0.2 to 2.5 kHz (Verbeek & McGee, 1995); the simulated streamer comprises 60 channels with 1-m spacing and minimum offset of 13 m. A realistic level of band-limited random noise has been added to the data; namely, the signal-to-noise ratio, computed with respect to the seafloor reflection amplitude, is equal to 50. Note in Fig. 1b how the strong P-wave velocity gradient determines a compression of the time delay among reflections at the longest offsets, which makes it difficult to accurately use moveout-based velocity estimation tools. The broad move-

out semblance maxima (Fig. 2) produce uncertainties in the velocity picking that translate into a broad range of possible interval P-wave velocity profiles; such variability is in general beyond a cycle-skipping safe domain (Virieux & Operto, 2009; Fichtner, 2011; Aleardi et al., 2016), and suggests that move-out velocity analysis is not a robust tool to obtain a starting P-wave model for local-search FWI. In the absence of reliable Cone Penetrometer Tests (CPT) and/or core-logs, the starting S-wave velocity and density profiles would also be derived from this P-wave model, further jeopardising the chance to converge to the global minimum of the multi-parameter objective function.

The latter is in fact a typical situation in engineering-scale seismic exploration and clarifies the potential benefits of a seismic inversion strategy that reduces the dependency upon the initial state of information. In the next sections, we demonstrate that, although the inherent sensitivity limitation of this kind of data cannot be overcome, our stochastic approach can still provide a robust solution when a wrong velocity trend is used to build the starting model search range.

2.2 Proposed genetic algorithm-based strategy

Stochastic optimisers like the genetic algorithm (GA Goldberg, 1989) represent a compromise between the systematic exploration of the model space and the exploitation of the current state of information about the physical model (Sambridge & Mosegaard, 2002); although more robust to cycle-skipping than deterministic FWI (Sajeva et al., 2016), they can similarly suffer from local-minima entrapment, depending on the model space dimensionality and the nature of the objective function (Sajeva et al., 2017).

In this paper, we introduce relevant changes to a classic evolutionary algorithm framework, in order to attenuate the bias inherited from ill-characterised a-priori distributions, and reduce the effective size of the model space. The proposed strategy is based on the genetic algorithm developed by Vardy (2015), adapted to the multi-parameter FWI of multi-channel data (Fig. 3). The subsurface is assumed to be horizontally stratified (Fig. 1), and each isotropic elastic layer is parametrised in terms of P-impedance (Z), Poisson's ratio (ν) and density (ρ) (Debski & Tarantola,

1995; Igel et al., 1996; Provenzano et al., 2017). The inversion workflow can be divided into 3 stages:

(i) In the first stage, the goal is to obtain a high-fidelity P-wave velocity model, robust to inaccurate a-priori information. An initial population of P-wave profiles is generated within a search-window built around the semblance-derived interval velocities. Unlike a classic GA, which performs a purely random exploration of the model space, here each individual of the initial population results from the superposition of a random long-wavelength component and a high-frequency perturbation, defined according to the frequency band of the data, and the minimum expected velocity. For each model, the multi-channel seismogram is computed using a homogeneous-layer method (Schmidt & Jensen, 1985; Schmidt & Tango, 1986.) and the value of the objective function is calculated. The following generation is then populated using a stochastic remainder criterium (Vardy, 2015); all models with fitness better than average are propagated to the next generation and the remaining individuals are randomly selected among the entire population. The survivors are crossed-over and mutated according to user-defined crossover and mutation probabilities. The long- and short-wavelength components of the model are completely decoupled, with the crossover and mutation elements of the GA operating on each independently.

(ii) After convergence is attained, the data are inverted for the elastic properties (Z, ν, ρ) . The genetic algorithm operates on the multi-parameter elastic space, preconditioned by the robust P-wave velocity model obtained in the previous stage. Shear-wave velocity and density trends, which can't be constrained independently by single-component marine seismic data alone (Operto et al., 2013), are derived from the long wavelengths of the P-wave velocity profile, by using appropriate rock-physics relationships (Hamilton, 1970; Richardson & Briggs, 1993; Mavko et al., 2009). By contrast, the high-frequency, reflective component, of the elastic model is estimated from the offset-dependent seismic waveforms. The width of the search range is modulated by the local P-wave reflectivity; the higher the P-impedance contrast, the wider the range. The rationale is to bias the inversion towards regions where anomalies in the elastic properties are most probable: Poisson's ratio and density are expected to change where P-wave impedance changes (Hamilton, 1970; Mavko et al., 2009), i.e. at interfaces between sediment types. Thereby the effective

size of the model space is selectively reduced, thus improving the efficiency in high-dimensional parametrizations (Tarantola, 2005; Sajeve et al., 2016).

(iii) Multiple independent runs are performed, each starting from an independent random population of models (Sen & Stoffa, 1992; Vardy, 2015). This produces an ensemble of statistically independent solutions, from which the model parameters error boundaries can be computed, without the bias of genetic drift and model inter-dependency (e.g. Vardy, 2015). The process is iterated until the estimate of the median model is stable, as in Stoffa & Sen (1991). The aim of this process is to obtain a measure of the reproducibility of the solution rather than an importance sampling of the PPD, which is not achievable using a GA without further exploration of the model space (Stoffa & Sen, 1991; Sambridge, 1999; Aleardi & Mazzotti, 2017).

In the next section we provide experimental proof of the efficacy of the methodology on both synthetic and real data: the decoupled approach, is effective at retrieving the true P-wave velocity model even when it lies at the edges of the range, while the structural preconditioning improves the efficiency of the elastic inversion by reducing the size of the model space. Both synthetic data (Fig. 1) and a real case study are presented. We will hereafter refer to our proposed strategy as *DGA (Decomposed Genetic Algorithm)*. In analogy with Bayesian methods, the search domain will be referred to as a-priori probability density function (PDF).

3 IMPLEMENTATION AND RESULTS

3.1 Robust P-wave velocity estimation with constant density and shear properties

Here we compare the proposed DGA to a GA inversion with a traditional parametrisation, for the reconstruction of an accurate P-wave velocity model starting from a ill-constructed a-priori search domain. The data and the true elastic model are shown in Fig. 1. The search window is built around the interval P-wave velocity model derived from semblance velocity analysis (Dix, 1955), in purple in Fig. 2, which represents an underestimate of the velocity gradient of about 5 %. Hence, the true model is significantly offset from the centre of the uniform a-priori PDF.

The model is parametrised as a stack of 30 layers with a thickness of 25 cm each, down to a

depth of 7-m below the seafloor. Only P-wave velocity is inverted for, whereas Poisson's ratio and density are kept fixed at this stage to a uniform profile ($\nu = 0.48$ and $\rho = 1.5g/cm^3$). A population of 160 individuals sampled from the a-priori PDF evolve through 150 generations according to an objective function $o(\mathbf{m})$ based on the L1 distance between the true data $\mathbf{r}(t)$ and the synthetic data $\mathbf{s}(t)$, computed for the model \mathbf{m} (Menke, 1989):

$$o(\mathbf{m}) = \sum_{j=1}^M \sum_{i=1}^N |r_{i,j} - s_{i,j}(\mathbf{m})| \quad (1)$$

where M is the number of traces and N is the number of time samples per trace. In this experiment, we compare the results obtained by computing the L1 residuals on *a)* the real waveform and *b)* its instantaneous phase modified according to Jimenez-Tejero et al. (2015). This is the inverse tangent of the ratio between the absolute value of the Hilbert transform $\mathbf{h}(t)$ of the trace and the real waveform $\mathbf{w}(t)$:

$$\phi(t) = \tan^{-1} \frac{|\mathbf{h}(t)|}{\mathbf{w}(t)} \quad (2)$$

The objective function computed on the the modified instantaneous phase (hereafter referred to as *MIP*) is independent from the waveform amplitude, and has proven in deterministic FWI to be beneficial for the inversion of data lacking low frequencies and acquired with short streamers (Jimenez-Tejero et al., 2015; Provenzano et al., 2017).

The DGA explores the model space by explicitly decomposing each random subsurface profile into a slowly-varying component, in the order of the dominant propagated wavelength ($\geq \lambda_{dom}$), and an independent high-frequency perturbation, in the order of the tuning thickness for the maximum frequency contained in the data ($\simeq \lambda_{min}/4$). This is achieved by generating two random series of chromosome values (i.e. P-wave velocity per layer), with correlation lengths respectively equal to λ_{dom} and $\lambda_{min}/4$, and superimposing them to create the broadband subsurface model (Fig. 4). For the P-wave velocities and source bandwidth of this test, the correlation lengths of the short and long wavelength components are respectively 0.25 and 1.25 m (Table 1). The decomposed approach is taken in both the sampling of the starting random population from the search range, and in the mutation and crossover through the generations. High mutation rates and relatively low crossover probabilities are used to enhance the explorative nature of the algorithm, and

	One parameter (V_p)	Elastic (Z, ν, ρ)
L(m)	1.25	-
S(m)	0.25	0.25
Number of variables	30	90
Mutation prob.	0.2	0.001
Crossover prob.	0.4	0.6
Number of individuals	160	320
Number of generations	150	150
Number of runs	50	50

Table 1. DGA inversion parameters. User-defined genetic algorithm parameters for the first-stage P-wave velocity inversion, and the following preconditioned simultaneous elastic inversion.

prevent from earlier convergence to local minima (Sen & Stoffa, 2013). The process thus accounts for the dual nature of the subsurface properties the seismic data are sensitive to, i.e. kinematic and reflective (Mora, 1980; Jannane, 1989). By contrast, in a conventionally parametrised GA the reconstruction of the broadband earth model results from random mutation and crossover operating on each layer individually. Unlike the DGA, the model samples of the GA are high-variance profiles clustered around the centre of the search domain, and are in fact more likely to produce geologically unrealistic features (Fig. 4).

In Figs. 5 and 6, we compare the median model and the 66 and 95 % solution confidence limits obtained from 50 independent inversion runs. The variation band of minimum and average L1 data misfit across the generations is also shown. The results show that the spectrally-decomposed algorithm outperforms the conventional parametrisation in attenuating the bias of the starting model: regardless the seismic attribute used, the true model is in fact included in the 95 % confidence limit of the DGA solution (grey shaded area in Figs. 5 and 6). However, the median model of the DGA waveform-based inversion is offset from the true P-wave profile, and the reproducibility of the solution is poor (Fig. 5). The MIP-based misfit functional (Jimenez-Tejero et al., 2015) ensures

more stable results (Fig. 6), proving a higher sensitivity to mid-to-long wavelength changes in the model, and lower liability to cycle skipping. In contrast, the waveform based objective function strongly suffers from local minima entrapment, because of the high non-linearity of the objective function with respect to the P-wave velocity trends (Virieux & Operto, 2009; Operto et al., 2013), and the mid-wavelength sensitivity gap due to the limited bandwidth and short offset of the data (Jannane, 1989). Therefore, the modified model exploration strategy is effective at attenuating the footprint of inaccurate a-priori information, but only if combined with an appropriate objective function.

By decomposing the P-wave velocity model into independent long and short components, and using a misfit criterium robust to cycle skipping, the inaccuracy in the starting model has been compensated for. Also, the model heterogeneities have been correctly located. The next step is to use this result to precondition the high-resolution multi-parameter elastic inversion.

3.2 Structure-preconditioned elastic inversion

Here we exploit the information contained in the estimated P-wave velocity model, in order to guide the inversion for the elastic properties. The model is parametrised in terms of P-impedance (Z), Poisson's ratio (ν) and density (ρ) (e.g. Debski & Tarantola, 1995; Igel et al., 1996; Provenzano et al., 2017). No independent constraint on the shear and density macro-model is posed by the single-component, limited offset data. So, in the absence of independent geological and geotechnical information, a sensible relationship with the P-wave velocity is needed to derive the elastic starting model. We make the assumption that such a relationship is available in our synthetic test, and is representative only of the long-wavelength component of the model. The high-wavenumber component, on the other hand, varies independently for each parameter, simulating changes in lithology and/or fluid saturation (Igel et al., 1996; Mallick & Dutta, 2002); such anomalies are the target of the elastic inversion, and are estimated entirely from the offset-dependent reflected wavefield.

The high-dimensionality of the multi-parameter problem determines a rapid increase of the

model space volume with the range width, hence of the number of model evaluations needed to

identify and sample its high-fitness region (Tarantola, 2005; Sajeve et al., 2016, 2017). In our specific test, each elastic layer is described by a triad of independent parameters (Z , ν and ρ), for a total of 90 degrees of freedom. It can be therefore beneficial to reduce the volume of the model space by selectively narrowing the search domain. For this purpose, we further exploit the information contained in the P-wave velocity profile to precondition the elastic inversion. The exploration of the elastic model space is biased towards model heterogeneity locations identified by regions of contrasting P-wave velocity, from the results of the first inversion stage.

The preconditioned search range for either ν and ρ , for each depth, is compactly defined as:

$$R = F(Vp_{sm}) \pm w_0 p \quad (3)$$

where:

$$p = \frac{\left| \frac{\partial^2 Vp}{\partial d^2} \right|}{\max \left(\left| \frac{\partial^2 Vp}{\partial d^2} \right| \right)} \quad (4)$$

the search range R is thus obtained from the smooth P-wave velocity Vp_{sm} using the rock-physics relationship F ; the half-width w_0 can be modulated by the second derivative of Vp , computed with respect to the depth d , and normalised to one. In Fig. 7 we compare the state of information available from the move-out based interval acoustic velocities with the one from the FWI P-wave profile; the latter allows us to build a more accurate multi-parameter search window, that reduces the risk of ruling out the true model from the a-priori model distribution.

The inversion parameters are summarised in table 1. Compared to the Vp-stage, we use a lower mutation rate, a higher crossover probability and a higher number of individuals per generation, to account for the higher number of unknowns (Stoffa & Sen, 1991; Sen & Stoffa, 1992). In Figs. 8 and 9, we show the inversion results and the marginal confidence intervals for the elastic inversion, respectively with and without range-width modulation. The confidence limits in both case are a high-fidelity representation of the elastic model, despite the low sensitivity of limited-offset marine data to shear properties variations, within the narrow Poisson's ratio range of shallow sediments (Mallick & Dutta, 2002; Provenzano et al., 2017). However, the fully-preconditioned test, with range modulation, produces solution confidence regions with better defined shear and density heterogeneities, especially in the deeper parts of the model.

In Fig. 10 the synthetic seismogram for the final FWI-model is overlaid to the real one, and the offset-dependent L1 misfit is plotted for each DGA stage. It is worth pointing out that the Vp-model, although obtained via instantaneous phase inversion, is responsible for a significant reduction of the waveform misfit, especially at the far offsets. The final misfits for the elastic models obtained with the two preconditioning techniques are similar; despite the higher misfit in some of the farthest channels, the fully-preconditioned solution has a higher fitness value, thanks to the better match at the higher-energy shortest offsets.

With a view to reducing the size of the model space, the range-width preconditioning will be key in the inversion of the real case study, where the presence of a 50 cm thick gas-saturated layer requires the inversion to explore a wide range of elastic moduli values in a thick spatial parametrisation.

3.3 Identification of shallow weak layers

3.3.1 Acquisition design and background information

Here we apply the elastic FWI to two UHF multi-channel seismic datasets acquired on a marine slope prone to shallow landsliding, in the Sør fjorden side-fjord near the town of Finneidfjord (Norway). The extensive suite of high frequency geophysical, geotechnical and geological data in the study area (e.g. Steiner et al., 2012) identifies a composite 50 cm thick clay-rich bed with low stiffness, low density and high overpressure ratio that lies at shallow depth within the background silty-clay sediments (Vanneste et al., 2012; Vardy et al., 2012; Vardy, 2015). This layer has been recognised as the failure plane for multiple submarine landslides from the last few decades and is thus referred to as *event bed* (L’Heureux et al., 2012; Steiner et al., 2012; Vanneste et al., 2012, 2015; Vardy et al., 2012). The saturation state of the event bed changes across the basin, from a water-saturated zone in the north to a gas-bearing area to the south (Vardy et al., 2012; Morgan et al., 2014).

The seismic source is a Boomer wide-band electro-acoustic plate with an effective bandwidth spanning from 0.2 to 2.5 kHz. The far-field signature has been measured during acquisition, and used as source wavelet in the inversion. The acquisition system is a 60-channel streamer with 1.0

m group spacing and maximum offset equal to 72 meters. A single receiver group has a length of 1 m and is made up by 7 elements, and both source and receiver group wavenumber filters have been included in the modelling

The inversion datasets at the two locations are supergathers obtained by stacking 15 adjacent CDPs (common depth point) gathers with 1m spacing, in order to attenuate the random noise energy. Data pre-processing is limited to muting the direct arrival and band-pass frequency filtering in the desired modelling bandwidth (0.2-2.0 kHz). The receiver ghost reflections are a strong source of coherent noise in the data (Fig. 11), particularly at site A, where the seafloor ghost reflection has higher energy than the event bed reflection and the respective traveltimes intersect. We include the receiver ghosts in the forward model by integrating the one dimensional solver with a custom-built frequency-wavenumber filter that accounts for the strong variation of the streamer depth and sea-surface reflection coefficient with offset (Provenzano et al., 2017).

Because of the availability of a reliable ground-truth, the challenging nature of the seismic data and the geohazard implications, this is an excellent case study to test the potential of UHF seismic inversion.

3.3.2 *Elastic FWI and ground-truthing*

We apply the inversion at two key locations, outside (Site A) and inside (Site B) the gas front (Fig. 11), with the aim to locate and characterise the event bed, and quantify the changes in partial gas saturation. P-wave velocity and bulk density measurements from a *Multi Sensor Core Logger (MSCL)* core proximal to Site A (Fig. 11), provide the low-frequencies to build a reliable starting model; therefore the computational effort in this section will be devoted to the identification of geohazard-relevant features. The one-dimensional approximation is justified by the almost plane-parallel geometry of the shallow reflectors in the pre-stack depth-migrated (PSDM) image (Fig.11). Preliminary analysis of the available reflection angle range suggests that, due to the short aperture of the data compared to the target depth, density and P-impedance can't be resolved independently (Provenzano et al., 2017), therefore a full elastic (Z , ν , ρ) multi-parameter inversion

would be heavily ill-posed. As shown in Igel et al. (1996) and Provenzano et al. (2016, 2017), a more appropriate parametrisation in this case is (Z, ν) .

Inversion parameters at site A are presented in Table 2. The relatively narrow range of expected values allowed for the simultaneous (Z, ν) inversion to converge to a satisfactory solution. The median model attains an excellent match with the MSCL acoustic impedance within the seismic resolution (Fig. 12), capturing the composite structure of the low-impedance anomaly between 3.5 and 4.0 m depth. The results suggest that the strongest heterogeneity at the event bed is the bottom interface, whereas the top one is probably a graded boundary at the seismic resolution. The Poisson's ratio model, on the other hand, does not contain important discontinuities, most probably because of the low-sensitivity of reflection data to changes in shear properties in the range of non-lithified sediments (≥ 0.49 ; Hamilton, 1970; Mallick & Dutta, 2002; Provenzano et al., 2017). In Fig. 13 we compare the real seismogram to the computed one for the best-fit model; note that the small amplitude negative polarity reflection associated with the event bed is correctly represented in the inversion, despite the strong receiver ghost, which overlaps the up-going reflection within a significant range of offset. The small reduction of normalised offset-dependent misfit between the starting low-frequency model and the FWI-solution, is explained by the low energy of the subsurface reflections compared to the primary and ghost seafloor reflections.

The inversion at site B is performed using the parameters summarised in Table 3. Because we want account for the possible presence of free gas, broader (Z, ν) search windows are required to allow for the inversion to converge close to the true elastic model; due to the gas saturation, P-impedance values close-to or lower-than the water column acoustic impedance are expected, and Poisson's ratio can span a broad range of values (Anderson & Hampton, 1980a; Ostrander, 1984; Tóth et al., 2014). Attempts to invert simultaneously Z and ν failed to converge to a meaningful solution, thus the two-stage preconditioned strategy is applied to reduce the size of the model space. The first stage of P-impedance inversion places the event bed between 7.5 and 8.0 m below the seafloor (*b.s.f.*); this model is then smoothed using a moving average filter with a correlation length of 50 cm ($\simeq \lambda/2$, Fig. 14), and used to precondition the range-width of the elastic inversion according to Eq. 3.2. The final model shows a drop of Z at 7.4 m b.s.f., with a 95% confidence

	One parameter (V_p)	Elastic (Z, ν)
S(m)	-	0.15
Number of variables	-	120
Mutation prob.	-	0.001
Crossover prob.	-	0.6
Number of individuals	-	420
Number of generations	-	100
Number of runs	-	50

Table 2. Site A inversion parameters. User-defined genetic algorithm parameters for the simultaneous elastic inversion.

interval reaching values under $600m/s \cdot g/cm^3$, correlated to a decrease in ν . The confidence intervals for ν are broad, and the solution for Z shows a probably non-physical long wavelength harmonic trend, as a consequence of the limited sensitivity of the short-offset reflection data in a relatively deep-water environment (Mallick & Dutta, 2002; Operto et al., 2013). Nevertheless, the FWI univocally identifies a shallow horizon with reduced bulk modulus, consistent with the presence of free gas in the pore space. The solution models after each stage account for a significant reduction of the offset dependent misfit in Fig. 15 compared to the initial state of information, and the final computed seismogram shows an excellent match with the real one.

3.3.3 *Can we quantify the free-gas content?*

As an example application, we use the FWI results to estimate a partial gas-saturation distribution in the sediment column. The presence of small amounts of free gas in the pore space is expected to produce a strong increase in the bulk sediment compressibility, having, on the other hand, little effect on its shear modulus (Mavko et al., 2009). Therefore, a drop of P-wave velocity associated with a decrease of Poisson's ratio is expected (Aki & Richards, 2002). Also, gas-bubble resonance

	One parameter (V_p)	Elastic (Z, ν)
S(m)	0.2	0.2
Number of variables	35	70
Mutation prob.	0.01	0.001
Crossover prob.	0.6	0.6
Number of individuals	320	500
Number of generations	120	150
Number of runs	10	50

Table 3. Site B inversion parameters. User-defined genetic algorithm parameters for the first-stage P-wave velocity inversion, and the following preconditioned simultaneous elastic inversion.

produce frequency-dependent changes in attenuation and P-wave velocity, which are significant at frequencies higher than the characteristic resonance frequency of the dominant bubble size (Anderson & Hampton, 1980a; Tóth et al., 2015).

Under the assumption that bulk mechanical effects dominate in our frequency band (0.2–2.5 kHz; Riedel & Theilen, 2001), we apply the geo-acoustic model by Anderson & Hampton (1980b) to estimate the partial gas saturation (Tóth et al., 2014). The model accounts for the increase of compressibility due to the presence of gas in the pore space, with respect to a water-saturated sediment at a given hydrostatic pressure. The model predicts the three-phase medium bulk modulus (K_m), and the shear modulus (μ), from which the (Z, ν) couple at each depth can be derived assuming an elastic isotropic mechanics (Mavko et al., 2009). The partial gas-saturation value is obtained by iteratively minimising the difference between the FWI-model and the predicted one.

Fig. 16 shows the results obtained at site B by fitting the FWI results within the confidence intervals, and compares the FWI-solution with the elastic properties predicted by the geo-acoustic model. A free-gas anomaly is placed at 7.5 m below the sea-floor, with a partial gas saturation confidence area in the order of 0.03%; this in good agreement with previous results obtained independently at the same site employing different high-resolution seismic sources with dissimilar

inversion techniques (Vanneste et al., 2013; Morgan et al., 2014). The same procedure applied to site A resulted in a gas saturation one order of magnitude lower (Fig. 17).

3.4 Discussion

The real case study demonstrates stable results, in excellent agreement with the geotechnical ground-truth at the seismic resolution. This makes a strong case for the use of seismic data as a remote characterisation tool for decimetric-scale features relevant to geohazard. In general, even when the final solution confidence intervals are broad, as in site B, the stochastic inversion succeeds at improving the a-priori state of information about the subsurface, in a purely data-driven way. In Site A, the solution for P-impedance reproduces the MSCL V_p data, almost perfectly within the seismic resolution, constituting a virtual *in-situ* elastic log. In site B, our structure-preconditioned strategy is fundamental to obtain convergence in the simultaneous multi-parameter inversion. The (Z, ν) model univocally identifies a shallow horizon showing a typical signature of gas saturation, as expected from the available independent data.

In the real data example, the availability of a P-wave velocity profile, measured on a core proximal to the inversion site, allowed us to design an accurate search range for the stochastic optimiser. When this is not the case, low-resolution P-wave models obtained from the reflection kinematics (e.g. from NMO analysis), can be used for the purpose. However, especially in sites with a strong shallow velocity gradient, inaccuracy in the semblance-derived starting model could bias the genetic algorithm away from the true broadband model. On the other hand, a uniform search range, between the maximum and the minimum expected velocities, significantly increases the number of samples required for an effective exploration of the model space (Tarantola, 2005), therefore reducing the chances of convergence within a feasible computing time (*curse of dimensionality*, e.g.; Sajeve et al., 2016, 2017). Thus, we suggest that reflection moveout analysis can be used as a quick method to narrow the range of possible earth models, and that this should be combined with an appropriate seismic inversion strategy. In the synthetic example, the proposed decoupled parametrisation of the P-wave velocity model, combined with a misfit criterium based

on the instantaneous phase (Jimenez-Tejero et al., 2015), proved to be able to compensate for ill-constructed search ranges, attenuating the bias of the starting model on the solution.

In the preconditioned elastic stage, a robust relationship among the long wavelength of the elastic parameters is only needed to build the search window, and can reflect the expected sediment type (Hamilton, 1970; Richardson & Briggs, 1993), or previous information about the recent geological history of the study area (e.g. Vardy et al., 2017). Detectable converted S-wave and post-critical reflections would probably allow us to constrain independently the shear properties long wavelengths, but this is often not the case in short-offset marine data (Kormendi & Dietrich, 1991; Igel et al., 1996; Vardy et al., 2017).

The elastic stage of reflection FWI aims at estimating the high-frequency elastic structures responsible for the offset-dependent seismic reflectivity, which are indicators of local anomalies in sediment fabric, lithology, or partial fluid saturation. The constraint posed by reflection data on the elastic parameters is highly hierarchical (Tarantola, 1986; Igel et al., 1996), namely higher for P-wave impedance, whereas independent density anomalies can only be detected if wide reflection angles are available ($> 40^\circ$; Provenzano et al., 2017). Sensitivity to differential changes of P- and S- waves in non-lithified, water-saturated media is also low, because they span a narrow Poisson's ratio range, with little footprint on the AVO response (Mallick & Dutta, 2002; Provenzano et al., 2017). This explains, in the synthetic example, the lower accuracy of the reconstructed shear and density profiles compared to the P-wave impedance result, and, in the real data, the absence of significant Poisson's ratio interfaces correlated to the event bed. By contrast, small amounts of gas in the pore space correspond to greater Poisson's ratio anomalies, as in site B (Ostrander, 1984; Mallick & Dutta, 2002).

The aforementioned sensitivity issues in the multi-parameter elastic space can in principle be quantitatively estimated from the posterior model ensemble as solution non-uniqueness. Several techniques have been developed in the literature in order to make the evolutionary optimiser a proxy to Bayesian statistics (e.g., Sen & Stoffa, 1992, 1996; Sambridge, 1999; Aleardi & Mazzotti, 2017). However, it is beyond the scope of this paper to address the issue of an effective importance sampling of the model space using a genetic algorithm. The approach of this work is to perform

multiple inversion runs, starting from independent random model populations (Sen & Stoffa, 1992; Vardy, 2015), in order to estimate the reproducibility of the solution without the bias of genetic drift and model inter-dependency (e.g. Vardy, 2015). In the real case study elastic inversion, 50 independent runs were spread across 6 nodes; each run took 16 hours on a 16-core 2.6 GHz node, for a total computing cost of about 5 days. The synthetic inversion example, despite the two-stage approach, had a similar computing cost, because of the narrower bandwidth, the lower number of layers and the fewer unknowns.

In the real case study, the partial gas saturation boundaries estimated from the elastic model confidence intervals are consistent with previous independent geophysical studies (e.g. Vanneste et al., 2013; Morgan et al., 2014). While the gas saturations at this site have not been measured in situ (through pressure coring, or similar), the consistency amongst different geophysical methods is promising, especially because of the potential destabilising effect of gas-pockets within near-seafloor beds (e.g. Vanneste et al., 2013). However, similarly to the cited works, the compressible-gas model used (Anderson & Hampton, 1980b) does not account for gas bubble resonance. As shown by Tóth et al. (2015), the validity of this assumption is highly dependent on the dominant gas bubble size, which exerts an important influence on apparent P-wave velocity dispersion and attenuation (Anderson & Hampton, 1980a). Such frequency-dependent effects are negligible only at frequencies lower than the gas bubble characteristic frequency (Wilkens & Richardson, 1998). Since the bubble size is not known to the accuracy required to rule out P-wave velocity dispersion at the upper end of the spectrum of our data ($\simeq 2.0 - 3.0\text{kHz}$), this approach could have underestimated the true gas saturation value, and should therefore be considered a lower bound.

4 CONCLUSIONS

We proposed a dedicated strategy for the pre-stack waveform inversion of ultra-high-frequency marine reflection data, based on a genetic algorithm with a carefully constructed model space, and demonstrated the potential of the method as a tool for the remote characterisation of decimetric thickness layers.

(i) We have demonstrated that a genetic algorithm optimisation is not inherently robust against inaccurate starting models, and requires appropriate model parametrisation and a careful choice of the objective function. A spectrally-decoupled exploration of the model space, combined with a complex-trace based objective function has been shown to increase robustness against inaccurate a-priori distribution, e.g. derived from inaccurate pickings in reflection moveout analysis.

(ii) We have also shown that this robust P-wave velocity model can be used to precondition the multi-parameter elastic inversion, in order to reduce the size of the model space in high-dimensionality parametrisations. This allows us to obtain a complex elastic model starting from little a-priori information.

(iii) A real case study has confirmed the potential of stochastic seismic inversion as a tool for the remote characterisation of decimetric-scale structures useful for shallow geohazard assessment. A sedimentary bed correlated to the failure depth of multiple landslides in the study area has been identified. Signatures of changes in its partial gas saturation have been detected in the elastic model. Within the seismic resolution and sensitivity, an excellent match with the ground truth has been obtained

The computing cost of this approach depends on the time used by a single forward model, and the number of forward models necessary for a satisfactory exploration of the model space. These factors still prevent stochastic optimisation from being applied to 2D/3D elastic FWI, in which the number of independent parameters can be in the order of thousands. Nevertheless, a set of 1D elastic inversions can be performed at selected locations, and used to inform the reconstruction of the lateral heterogeneity of the subsurface. Furthermore, such one-dimensional models can be interpolated to obtain a data-driven, accurate starting model for deterministic 2D/3D elastic FWI. The proposed strategy for engineering-scale FWI is thus a precious practical tool to complement information from bathymetry, sub-bottom profilers, cores and CPTUs for shallow geohazard assessment, reducing the need of expensive and time consuming geotechnical sampling campaigns in areas prone to shallow marine landsliding.

ACKNOWLEDGMENTS

The work presented here was funded through the SEABED consortium with additional funding through the International Centre for Geohazards (ICG). The authors would like to thank Antonis Zervos, Tim Minshull and Hector Marin Moreno for the fruitful discussions regarding inversion and geomechanics. We also thank Rene-Edouard Plessix, Mrinal Sen and Andrea Tognarelli for the useful comments, that significantly improved the quality of the manuscript. The field data preconditioning was performed using a combination of Landmark's ProMAX software, MatLab, and Seismic Unix. The forward modelling was performed using the MIT OASES algorithm. All other processing used custom-written algorithms. The authors acknowledge the use of the IRIDIS High Performance Computing Facility, and associated support services at the University of Southampton, in the completion of this work.

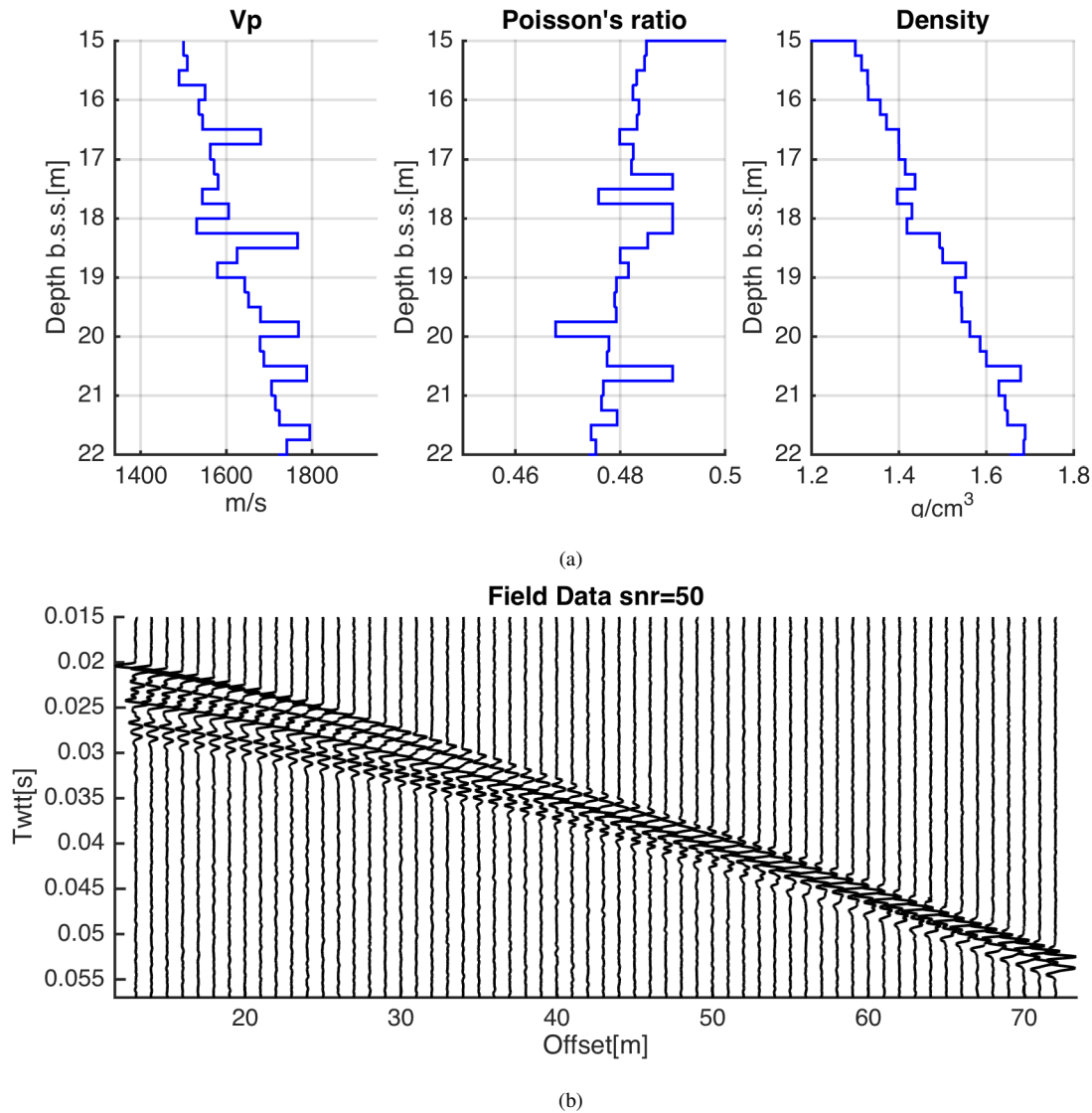


Figure 1. One-dimensional elastic model and synthetic data. In panel a) horizontally layered elastic model, parametrised as P-wave velocity (V_p), Poisson's ratio (ν) and density (ρ); depth relative to the sea surface. In panel b) common-shot multi-channel reflection seismic data simulating the acquisition in a shallow marine environment. The seismogram is computed using the *Oases* software (Schmidt & Jensen, 1985; Schmidt & Tango, 1986.), and contaminated with band-limited random noise; signal-to-noise ratio is equal to 50, computed with respect to the strongest reflection

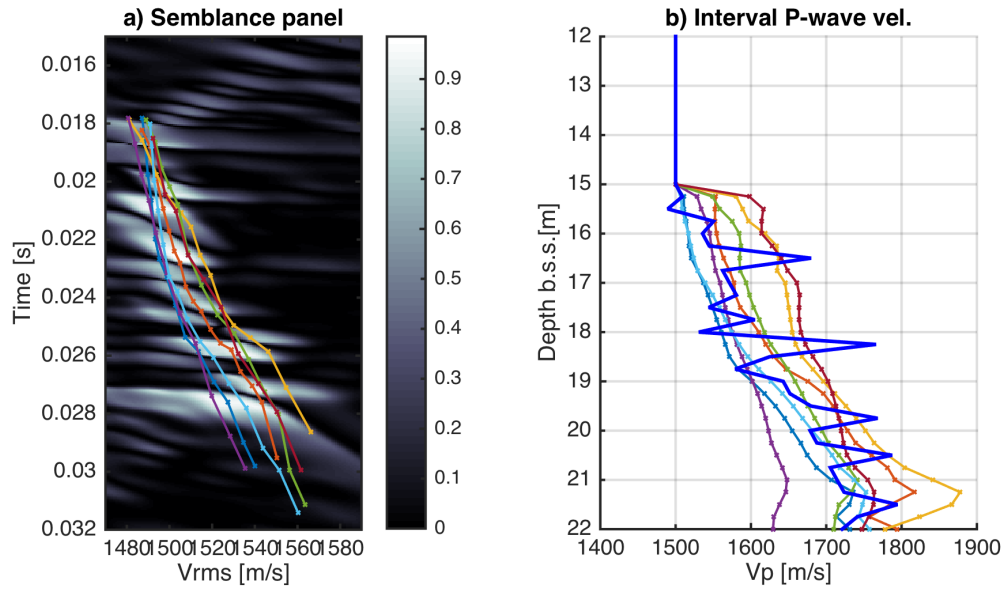


Figure 2. Deriving low-frequency P-wave velocity model from NMO analysis: panel a) stacking velocity semblance panel with possible V_{rms} pickings; panel b) interval P-wave velocity models (dotted-lines) derived using Dix (1955) equation from the V_{rms} , and true V_p model (solid blue).

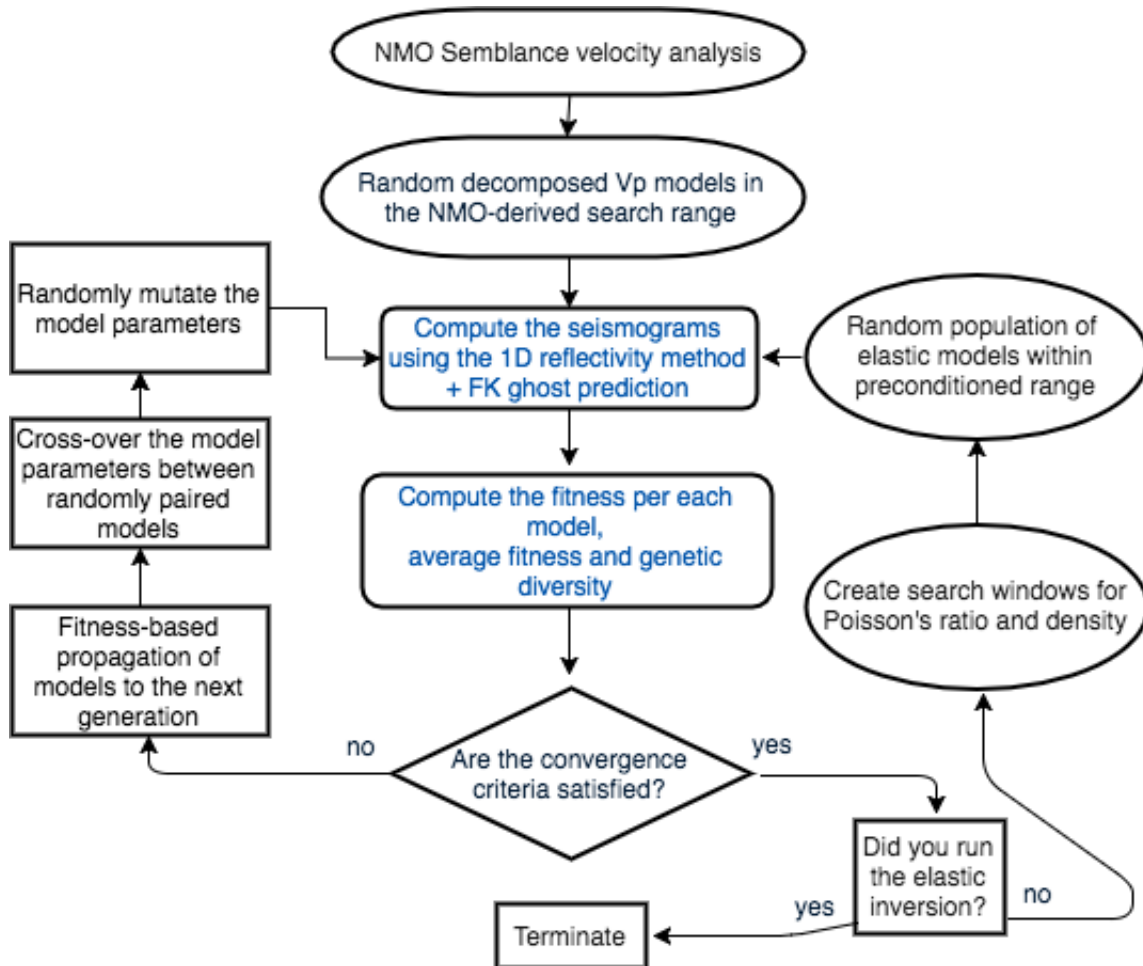


Figure 3. Inversion workflow. The flow chart summarises the proposed two-stage inversion strategy for the reconstruction of the multi-parameter elastic model. The steps for the computation of the models performance for each generation are highlighted in blue. The forward model is parallelised using openMP.

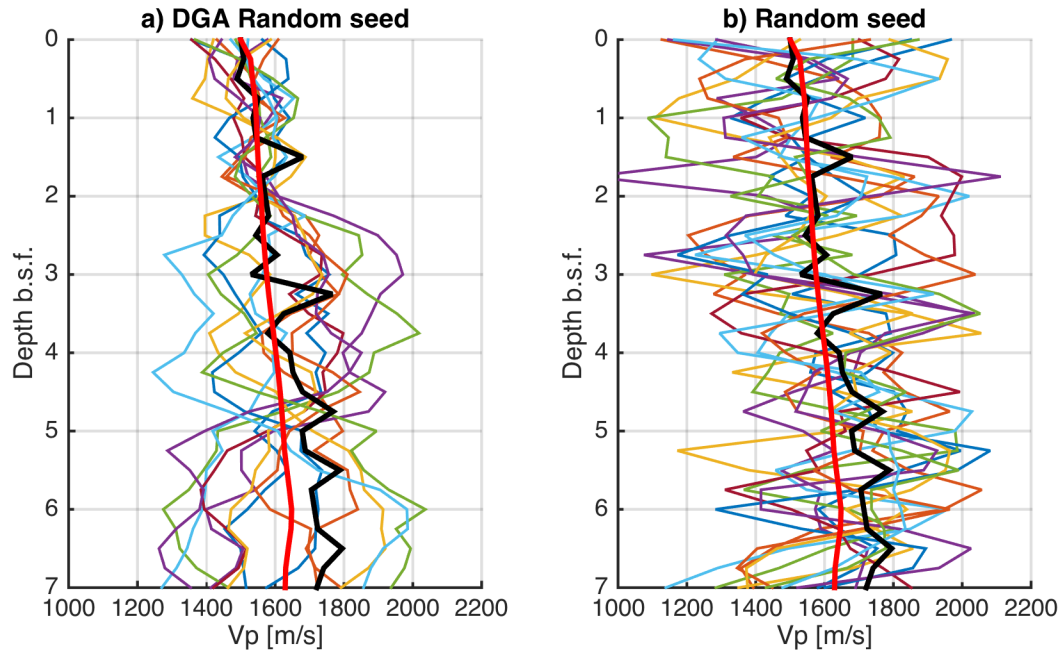


Figure 4. Random seeds In panel a) random models (thinner lines) generated by the decomposed algorithm within a search range designed around the semblance velocity model (thick red), and true Vp model (thick black). Correlation length for the high-frequency component is equal to the thickness of the individual layer ($0.25\text{cm} \simeq \lambda_{\min}/4$), and $\simeq 1\text{m}$ for the long component. In panel b) the random models are instead generated by sampling randomly the same Vp search window.

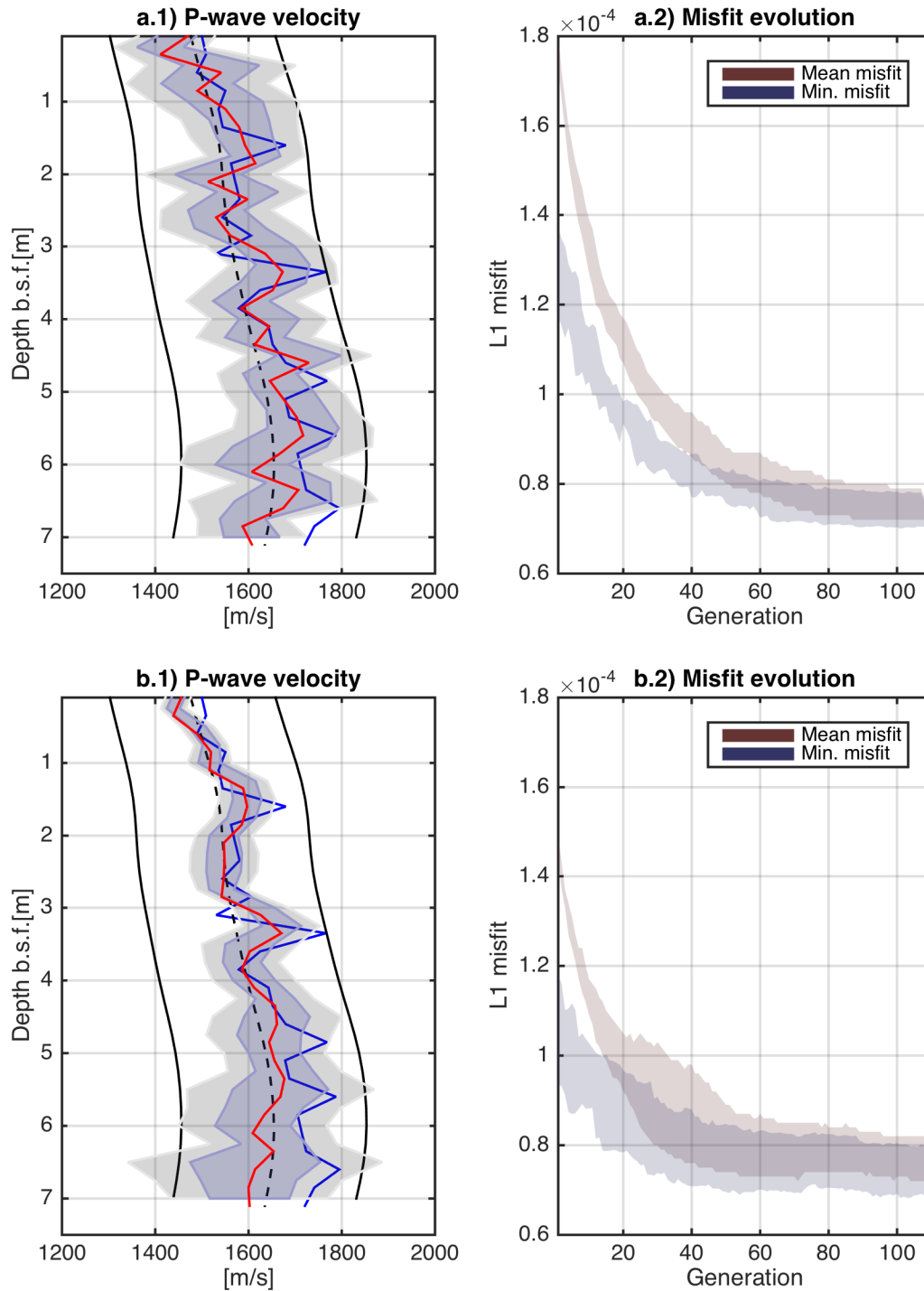


Figure 5. Vp inversion. Waveform L1 misfit functional. In panel a, results obtained using a GA with a conventional strategy; in panel b, results obtained using our DGA. True model (blue); median model (red) and shaded areas for the 66 (blue) and 95 (grey) % confidence intervals of the solution are computed from an ensemble of 50 independent realisations. The variability range of the average and minimum misfit evolution over the generations is shown. The final minimum misfit is lower for the DGA inversion, and the true model is included in the confidence interval. However, the high variability of the solution reveals a remarkable liability to cycle skipping.

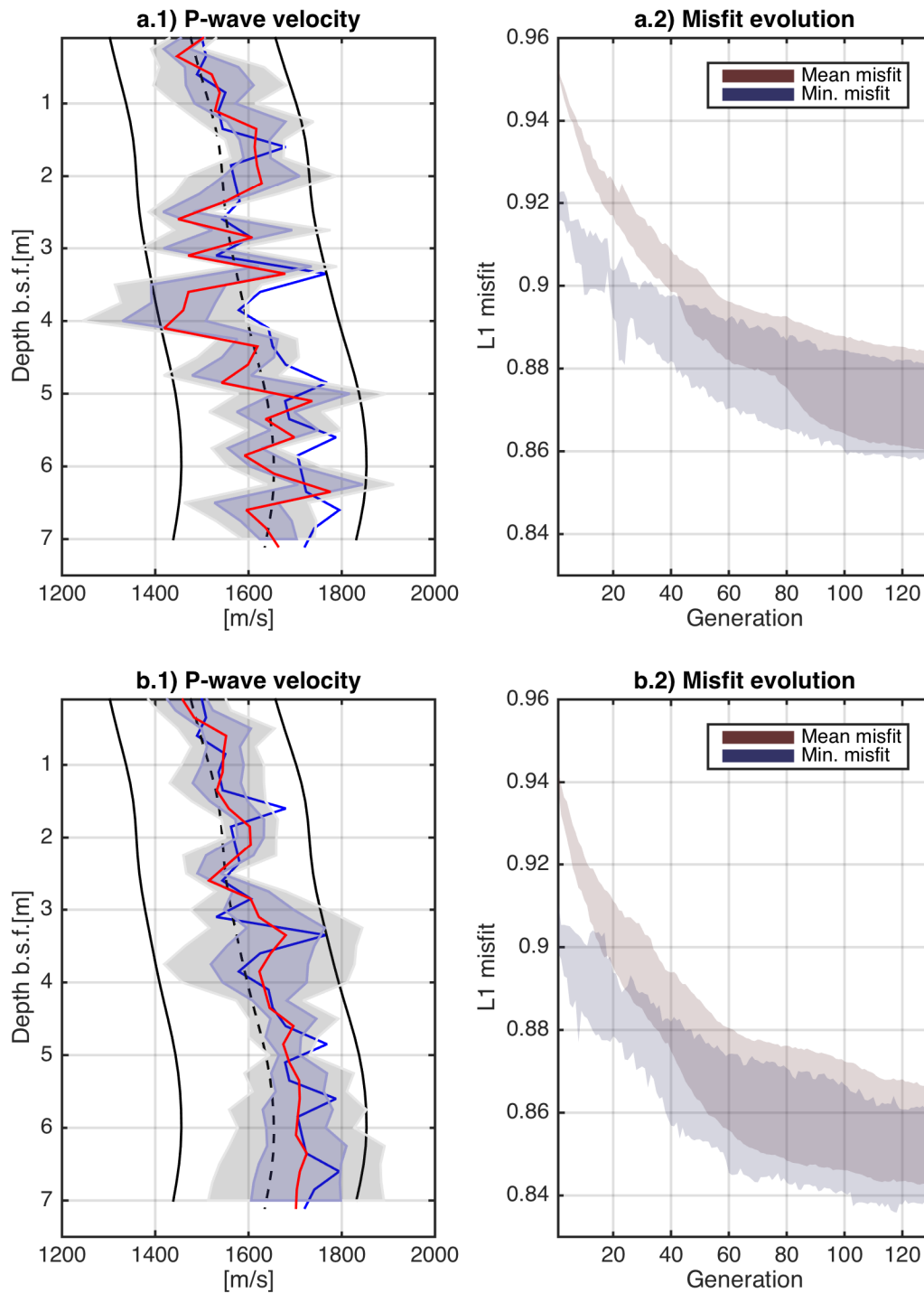


Figure 6. V_p inversion. Complex trace L1 misfit functional. In panel a, results obtained using a GA with a conventional strategy; in panel b, results obtained using our DGA. True model (blue); median model (red) and shaded areas for the 66 (blue) and 95 (grey) % confidence intervals of the solution are computed from an ensemble of 50 independent realisations. The variability range of the average and minimum misfit evolution over the generations is shown. Note how the DGA solution (panel b) is less dependent from the central model (dashed line) of the a-priori distribution, and that the final minimum misfit is lower than the

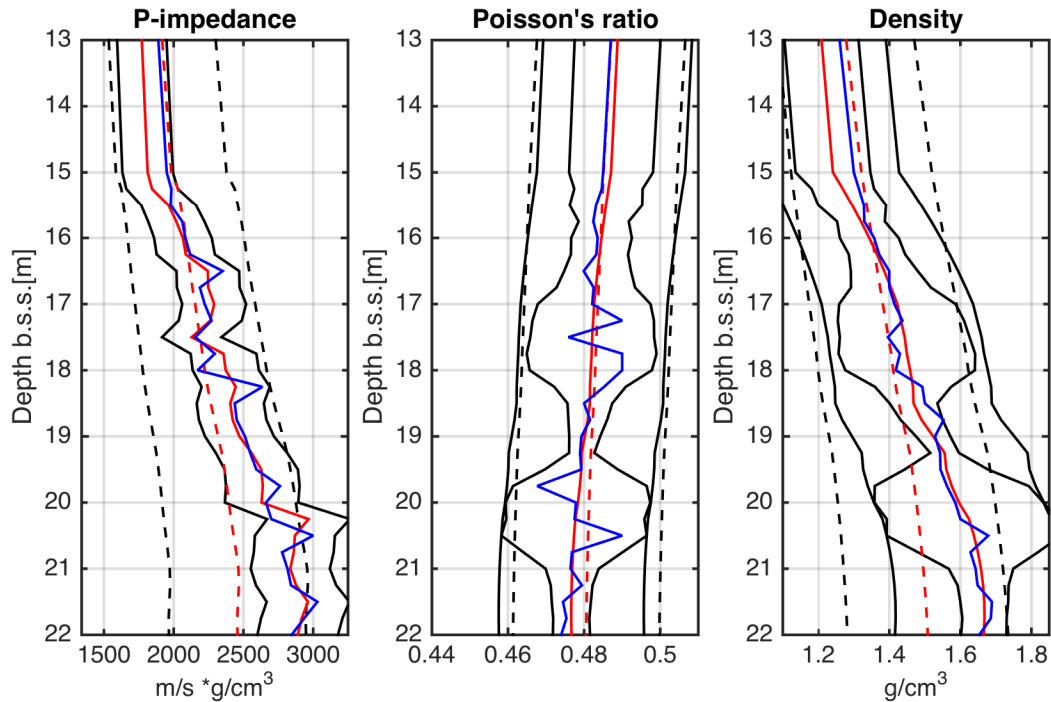


Figure 7. Advantage of using the P-wave velocity model to precondition the search window. Elastic model parametrised as (Z, ν, ρ) . Note that the Z model obtained at the first stage of DGA (solid red), allows us to build accurate estimates of the shear and density trends (also in solid red). The derived ranges (solid black) contain the true model (blue). Using the semblance P-wave model with the same empirical relationship (dashed red), increases the chances of excluding the true model from the search window (dashed black). In this example, this is particularly evident for density.

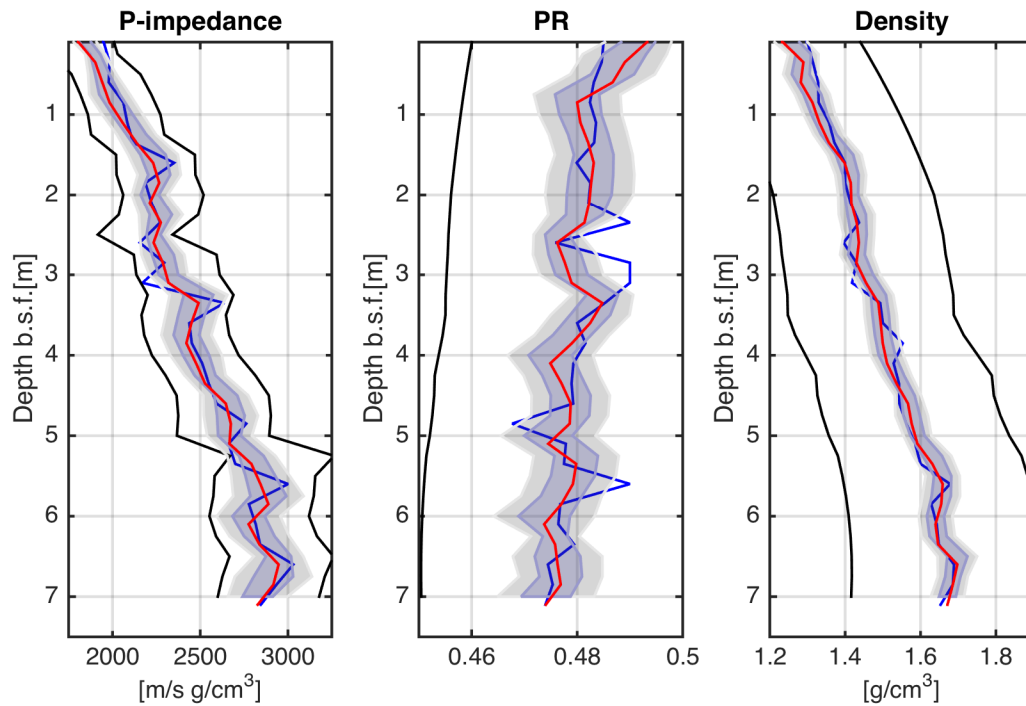


Figure 8. Elastic multi-parameter inversion with long-wavelength preconditioning. Median model (red) and 66 (blue) - 95 (grey) % confidence intervals obtained from 50 independent inversion runs; true model in blue and range boundaries in solid black. In this test, the preconditioning on Poisson's ratio and density is only in the long-wavelength of the P-wave velocity model obtained in the previous stage.

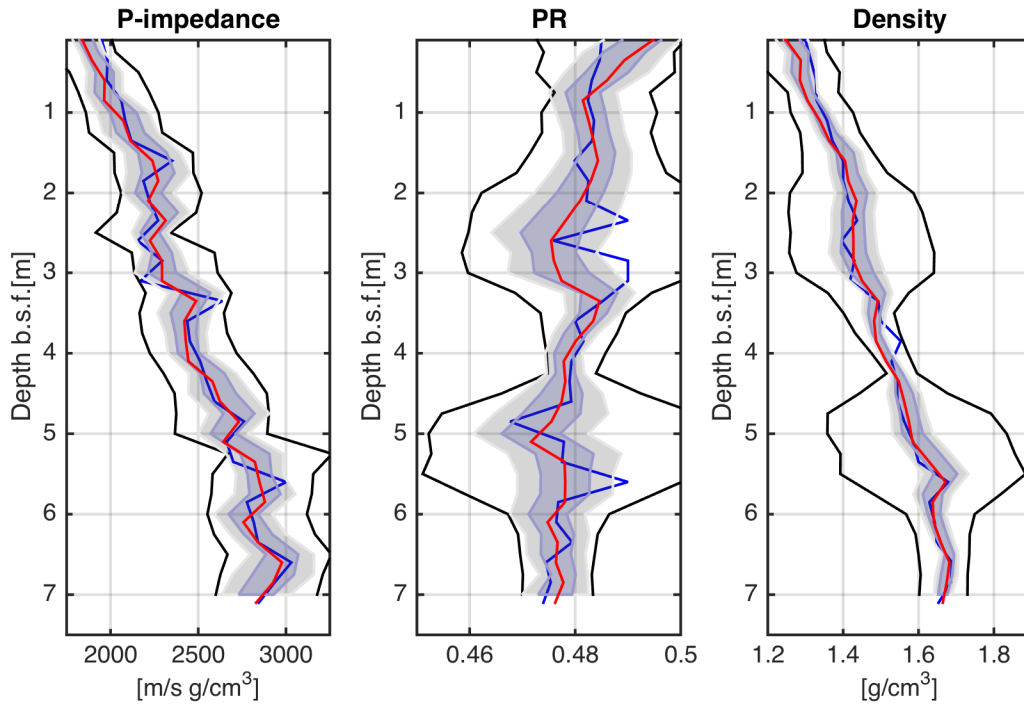


Figure 9. Elastic multi-parameter inversion with full preconditioning. Median model (red) and 66 (blue) - 95 (grey) % confidence intervals obtained from 50 independent inversion runs; true model in blue and range boundaries in solid black. In this test, full preconditioning is used, and the width of the search range is modulated by the local P-wave velocity model heterogeneities obtained in the previous stage.

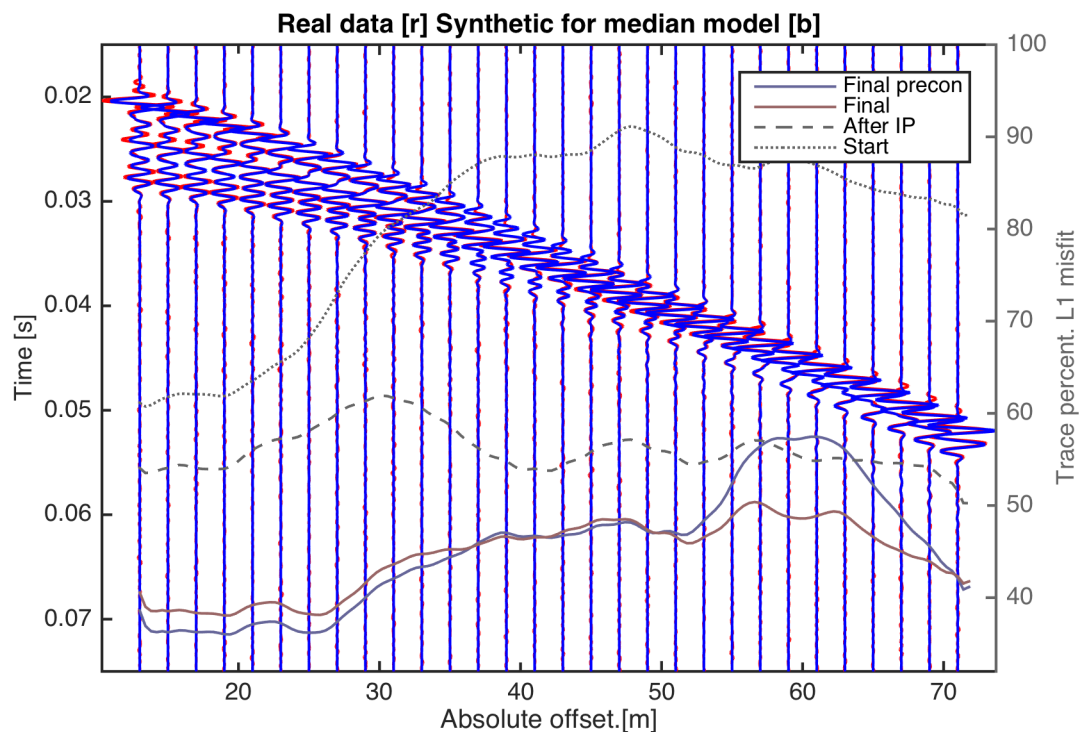


Figure 10. Two-stage elastic inversion offset-dependent misfit. Real seismogram (red), Synthetic seismogram (blue) for the median model after elastic FWI. Overlaid, offset-dependent trace-normalised L1 misfit for the starting NMO model (dash-dot grey), the final Vp model (dash grey), and the two median models, with and without range-width preconditioning (respectively blue and red).

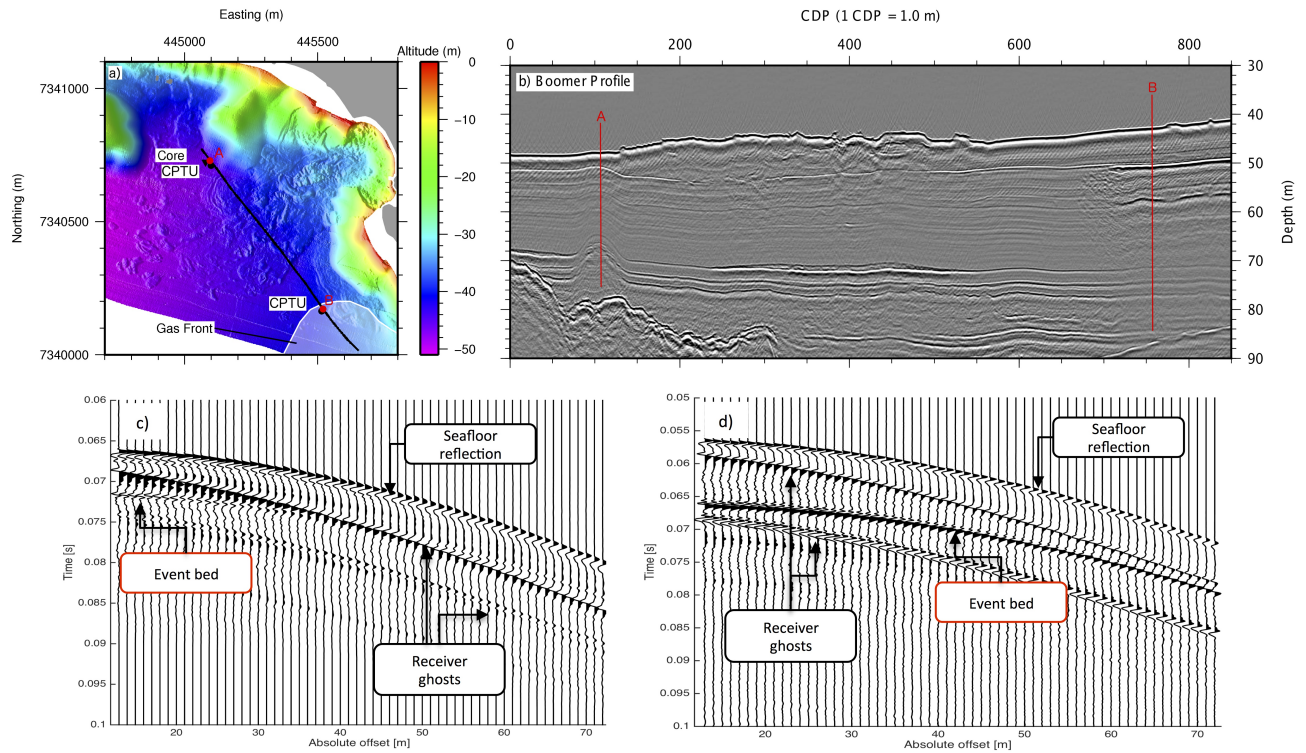


Figure 11. Panel a) bathymetric image of the study area, with location of the two CDP supergathers (site A and B). The seabed morphology clearly shows indicators of multiple marine landslides deposits. The gas front area is shaded. Panel b) migrated Boomer seismic line crossing the gas front. Panel c and d: Seismic gather respectively of site A and B. Note how the strong receiver ghost reflections cross the event bed reflection in site A.

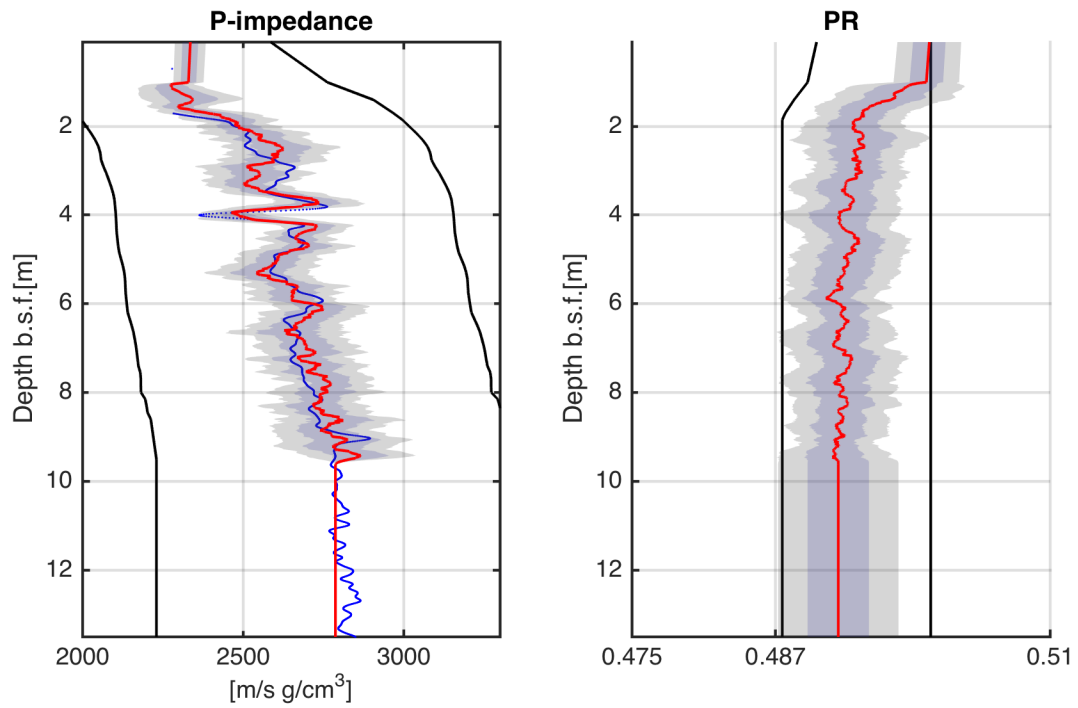


Figure 12. Site A elastic inversion results. Median (solid red) and 66 - 95 % confidence intervals (respectively blue and grey) obtained from 50 independent inversion runs; MSCL Impedance measured in-situ (blue); search boundaries (solid black lines).

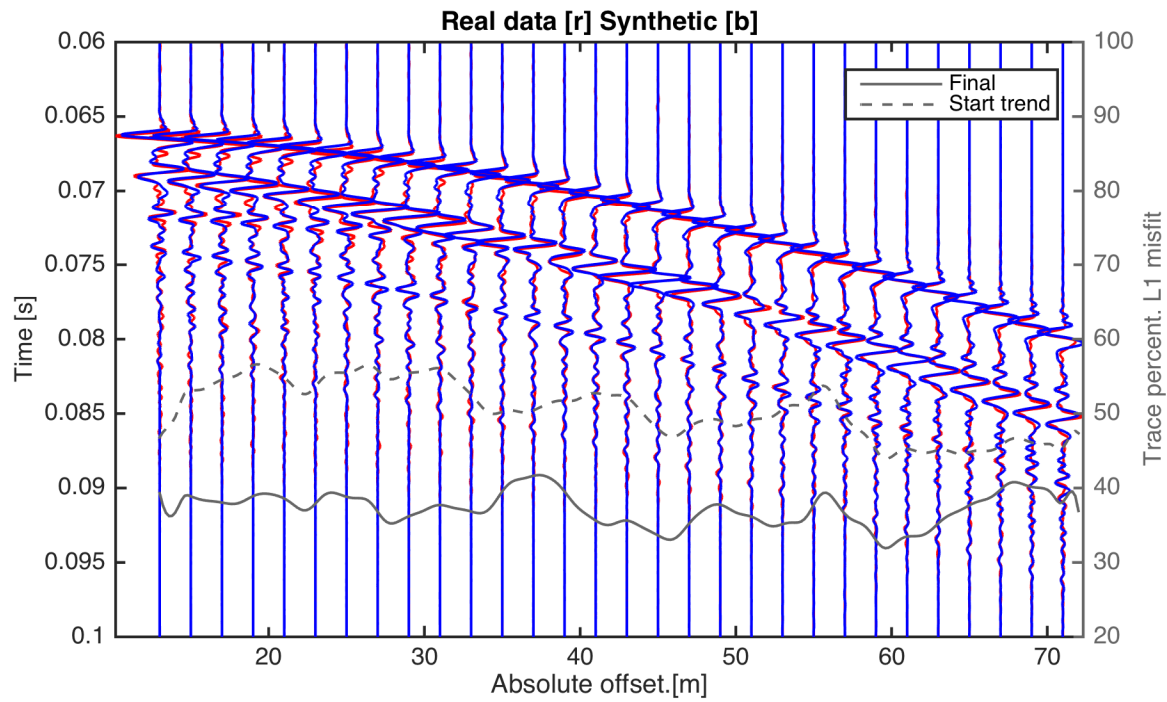


Figure 13. Site A elastic inversion offset-dependent misfit. Real seismogram (red), Synthetic seismogram (blue) for the median model after elastic FWI. Overlaid, offset-dependent trace-normalised L1 misfit for the starting low-frequency model (dash-dot grey) and the final FWI-model (solid grey).

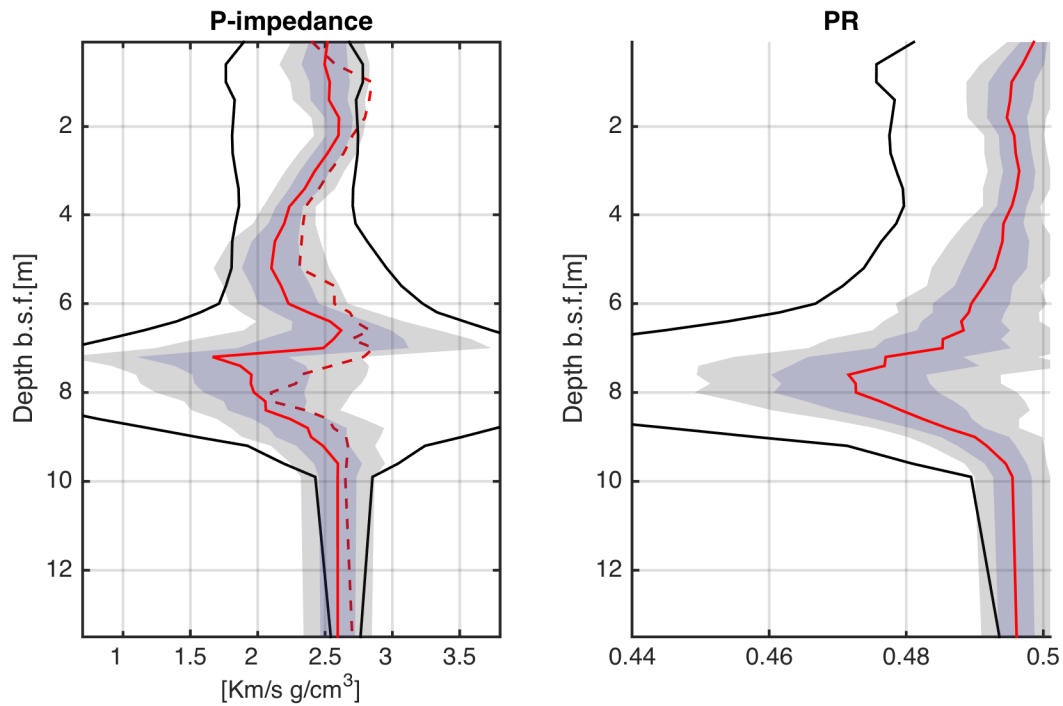


Figure 14. Site B elastic inversion results. Median model (solid red) and 66 - 95 % confidence intervals (respectively blue and grey) obtained from 50 independent inversion runs; search boundaries (solid black lines); the red dashed line is the smoothed P-impedance model from the single-parameter inversion, whose local rate of change is used to precondition the width of the search range for the elastic inversion.

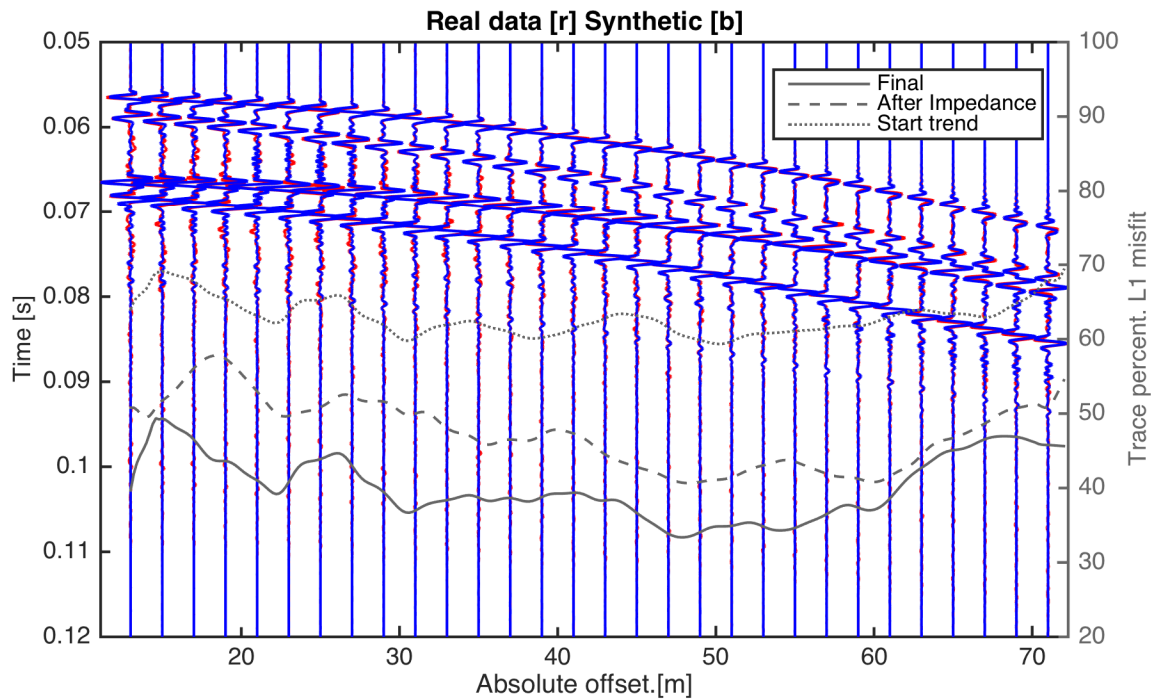


Figure 15. Site B elastic inversion offset-dependent misfit. Real seismogram (red), Synthetic seismogram (blue) for the final model after elastic FWI. Overlaid, offset-dependent trace-normalised L1 misfit for the starting low-frequency model (dash-dot grey), the final Vp model (dash grey), and the final FWI-model (solid grey).

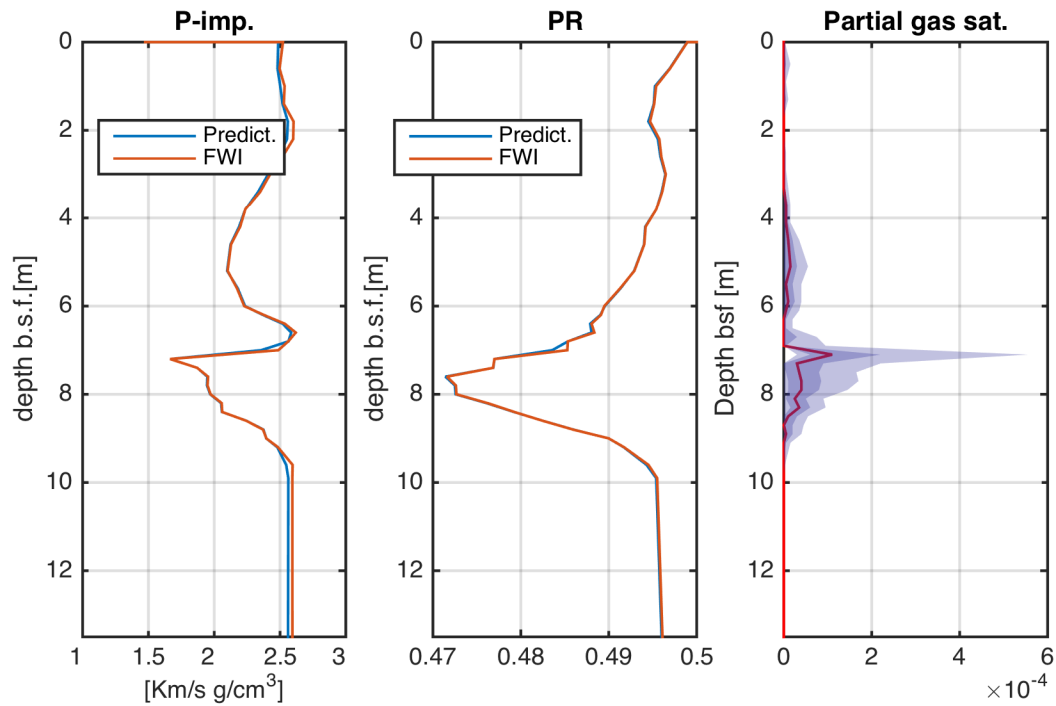


Figure 16. Site B. Partial gas saturation from Z and ν . P-impedance and Poisson's ratio predicted (blue) using Anderson & Hampton (1980b) model are compared with the FWI-solution (red). In the right panel, log-scale partial gas saturation estimated by fitting the median (red), and the 66 % (blue) and 95 % (grey) confidence limits.

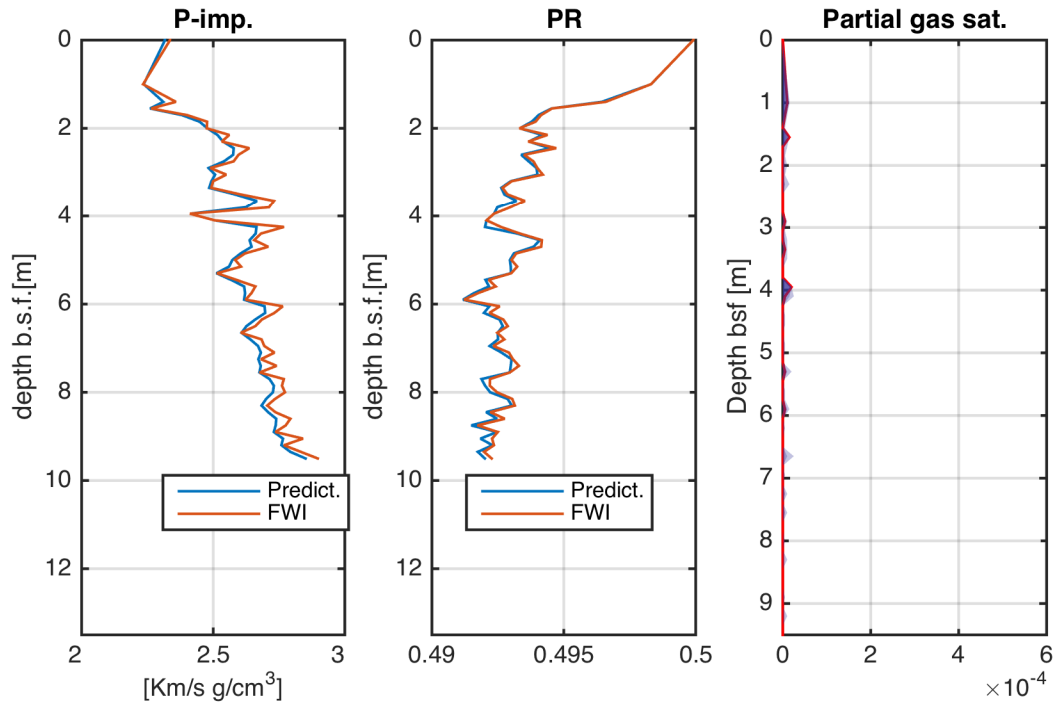


Figure 17. Site A. Partial gas saturation from Z and ν . P-impedance and Poisson's ratio predicted (blue) using Anderson & Hampton (1980b) model are compared with the FWI-solution (red). In the right panel, log-scale partial gas saturation estimated by fitting the median (red), and the 66 % (blue) and 95 % (grey) confidence limits. The same horizontal scale as in Fig. 16 is used keep consistency with the plot for site B.

References

- Aki, K. & Richards, P., 2002. *Quantitative Seismology*, University Science Books.
- Aleardi, M. & Mazzotti, A., 2017. 1D elastic full-waveform inversion and uncertainty estimation by means of a hybrid genetic algorithm-Gibbs sampler approach, *Geophysical Prospecting*, **65**, 64–85.
- Aleardi, M., Tognarelli, A., & Mazzotti, A., 2016. Characterisation of shallow marine sediments using high-resolution velocity analysis and genetic-algorithm-driven 1D elastic full-waveform inversion, *Near Surface Geophysics*, **14**, 449–460.
- Anderson, A. & Hampton, L., 1980a. Acoustics of gas-bearing sediments I. Background, *Journal of the Acoustical Society of America*, **67**, 1865–1889.
- Anderson, A. & Hampton, L., 1980b. Acoustics of gas-bearing sediments II. Measurements and models, *The journal of the acoustical society of America*, **67**, 1890–1903.
- Cevatoglu, M., Bull, J., Vardy, M., Gernon, T., Wright, I., & Long, D., 2015. Gas migration pathways, controlling mechanisms and changes in sediment acoustic properties observed in a controlled sub-seabed CO₂ release experiment, *International Journal of Greenhouse Gas Control*, **38**, 26–43.
- Clare, M. A., Vardy, M. E., Cartigny, M., Talling, P., Himsworth, M., Dix, J., Harris, J., & Whitehouse, R., 2017. Direct monitoring of active geohazards: emerging geophysical tools for deep-water assessments, *Near Surface Geophysics*, **15**, 427–444.
- Dagnino, D., Salláres, V., & Ranero, C. R., 2014. Scale and parameter-adaptive model-based gradient pre-conditioner for elastic full-waveform inversion, *Geophysical journal international*, **198**, 1130–1142.
- Debski, W. & Tarantola, A., 1995. Information on elastic parameters obtained from the amplitudes of reflected waves, *Geophysics*, **60**, 1426–1436.
- Dix, C., 1955. Seismic velocities from surface measurements, *Geophysics*, **20**, 68–86.
- Fichtner, A., 2011. *Full Seismic Waveform Modelling and Inversion*, Springer.
- Gholami, Y., Brossier, R., Operto, S., Prioux, V., Ribodetti, A., & Virieux, J., 2013a. Which parameterization is suitable for acoustic vertical transverse isotropic full waveform inversion?

- Part 2: Synthetic and real data case studies from Valhall, *Geophysics*, **78**, 107–124.
- Gholami, Y., Brossier, R., Operto, S., Ribodetti, A., & Virieux, J., 2013b. Which parameterization is suitable for acoustic vertical transverse isotropic full waveform inversion? Part 1: Sensitivity and trade-off analysis, *Geophysics*, **78**, 81–105.
- Goldberg, D., 1989. *Genetic Algorithms in Search, Optimization, and Machine Learning*, Addison Wesley Publishing Company, Reading, MA.
- Hamilton, E., 1970. Sound velocity and related properties of marine sediments, North Pacific, *Journal of Geophysical Research*, **75**, 4423–4446.
- Igel, H., Djikpesse, H., & Tarantola, A., 1996. Waveform inversion of marine reflection seismograms for P-impedance and Poisson's ratio, *Geophysical journal international*, **124**, 363–371.
- Jannane, M., 1989. Short Note. Wavelength of earth structures that can be resolved from seismic reflection data, *Geophysics*, **54**(7), 906–910.
- Jimenez-Tejero, C., Dagnino, D., Salláres, V., & Ranero, C., 2015. Comparative study of objective functions to overcome noise and bandwidth limitations in full waveform inversion, *Geophysical journal international*, **203**, 632–645.
- Kennedy, J. & Eberhart, R., 1995. Particle swarm optimization, *Proceedings of IEEE International Conference on Neural Networks*, **4**, 1942–1948.
- Kormendi, F. & Dietrich, M., 1991. Nonlinear waveform inversion of plane-wave seismograms in stratified elastic media, *Geophysics*, **56**(5), 664–674.
- L'Heureux, J.-S., Longva, O., Steiner, A., Hansen, L., Vardy, M. E., Vanneste, M., Haflidason, H., Brendryen, J., Kvalstad, T. J., Forsberg, C. F., Chand, S., & Kopf, A., 2012. Identification of weak layers and their role for the stability of slopes at Finneidfjord, northern Norway, *Submarine Mass Movements and Their Consequences. Advances in Natural and Technological Hazards Research*, **31**, 321–330.
- M. E. Vardy, M. V., Henstock, T., Clare, M. A., Forsberg, C., & Provenzano, G., 2017. State-of-the-art remote characterization of shallow marine sediments: the road to a fully integrated solution state-of-the-art remote characterization of shallow marine state-of-the-art remote characterization of shallow marine sediments: the road to a fully integrated solution, *Near Surface*

Geophysics, **15**, 387–402.

Mallick, S. & Adhikari, S., 2015. Amplitude variation with offset and pre-stack waveform inversion: a direct comparison using a real data example from the Rock Springs Uplift, Wyoming, USA, *Geophysics*, **80**(2), B45–B59.

Mallick, S. & Dutta, N., 2002. Shallow water flow prediction using prestack waveform inversion of conventional 3D seismic data and rock modeling, *The Leading Edge*, **21**, 675–680.

Mavko, G., Mukerji, T., & Dvorkin, J., 2009. *The rock physics handbook*, Cambridge U.P.

Menke, W., 1989. *Geophysical data analysis and inverse problems*, Academic Press INC.

Monrigal, O., Jong, I. D., & Duarte, H., 2017. An ultra-high-resolution 3D marine seismic system for detailed site investigation, *Near Surface Geophysics*, **15**, 335–345.

Mora, P., 1980. Inversion = migration + tomography, *Geophysics*, **54**(12), 1575–1586.

Morgan, E., Vanneste, M., & Vardy, M., 2014. Characterization of the slope-destabilizing effects of gas-charged sediment via seismic surveys, *Offshore Technology Conference-Houston*.

Operto, S., Prieux, Y., Ribodetti, A., Brossier, R., Metivier, L., & J. Virieux, 2013. A guided tour of multiparameter full waveform inversion with multicomponent data, *The Leading Edge*, pp. 936–947.

Ostrander, W., 1984. Plane-wave reflection coefficients for gas sands at non-normal angles of incidence, *Geophysics*, **49**(10).

Pinson, L., Henstock, T., Dix, J., & Bull, J., 2008. Estimating quality factor and mean grain size of sediment from high-resolution seismic data, *Geophysics*, **73**, G19–G28.

Provenzano, G., Vardy, M. E., & Henstock, T., 2016. Pre-stack waveform inversion of VHF marine seismic reflection data. A case study in Norway, in *Near Surface Geoscience 2016 – Second Applied Shallow Marine Geophysics Conference*.

Provenzano, G., Vardy, M., & Henstock, T. J., 2017. Pre-stack full waveform inversion of ultra-high-frequency marine seismic reflection data, *Geophysical journal international*, **209**, 1593–1611.

Richardson, M. & Briggs, K., 1993. On the use of acoustic impedance values to determine sediment properties, in *Acoustic classification and mapping of the seabed*, vol. 15.

- Riedel, M. & Theilen, F., 2001. AVO investigations of shallow marine sediments, *Geophysical prospecting*, **49**, 198–212.
- Rothman, D., 1985. Nonlinear inversion, statistical mechanics, and residual statics estimation, *Geophysics*, **50**, 2784–2796.
- Ruthenford, S. & Williams, R., 1989. Amplitude-versus-offset variations in gas sands, *Geophysics*, **54**(6), 680–688.
- Sajeva, A., Aleardi, M., Stucchi, E., & Mazzotti, A., 2016. Estimation of acoustic macro models using a genetic full-waveform inversion: Applications to the marmousi model, *Geophysics*, **81**, 173–184.
- Sajeva, A., Aleardi, M., Galluzzi, B., Stucchi, E., Spadavecchia, E., & Mazzotti, A., 2017. Comparing the performances of four stochastic optimisation methods using analytic objective functions, 1D elastic full-waveform inversion, and residual static computation, *Geophysical Prospecting*, **65**, 322–346.
- Sambridge, M., 1999. Geophysical inversion with a neighbourhood algorithm II. Appraising the ensemble, *Geophysical journal international*, **138**, 727–746.
- Sambridge, M. & Mosegaard, K., 2002. Monte carlo methods in geophysical inverse problems, *Reviews of Geophysics*, **40**(3), 1–29.
- Schmidt, H. & Jensen, F., 1985. A full wave solution for propagation in multilayered viscoelastic media with application to gaussian beam reflection at fluid-solid interfaces., *Journal of the Acoustic Society America*.
- Schmidt, H. & Tango, G., 1986. Efficient global matrix approach to the computation of synthetic seismograms., *Geophysical Journal Research Astronomical Society*.
- Sen, M. & Stoffa, P., 1992. Rapid sampling of model space using genetic algorithms. examples from seismic waveform inversion, *Geophysical journal international*, **108**, 281–292.
- Sen, M. & Stoffa, P., 1996. Bayesian inference, Gibbs’ sampler and uncertainty estimation in geophysical inversion, *Geophysical Prospecting*, **44**, 313–350.
- Sen, M. & Stoffa, P., 2013. *Global Optimization Methods in Geophysical Inversion*, Cambridge

- Steiner, A., L'Heureux, J.-S., Kopf, A., Vanneste, M., Longva, O., & Lange, M., 2012. *Submarine Mass Movements and Their Consequences*, chap. An In-Situ Free-Fall Piezocone Penetrometer for Characterizing Soft and Sensitive Clays at Finneidfjord (Northern Norway), Springer, Dordrecht.
- Stoffa, P. & Sen, M., 1991. Nonlinear multiparameter optimization using genetic algorithms: inversion of plane wave seismograms, *Geophysics*, **56**, 1794–1810.
- Stoker, M., Bradwell, T., Howe, J., Wilkinson, I., & McIntyre, K., 2009. Lateglacial ice-cap dynamics in NW Scotland: evidence from the fjords of the Summer Isles region., *Quaternary Science Reviews*, **28**, 3161–3184.
- Tarantola, A., 1984. Inversion of seismic reflection data in the acoustic approximation, *Geophysics*, **49**(8), 1259–1266.
- Tarantola, A., 1986. A strategy for nonlinear inversion of seismic reflection data, *Geophysics*, **51**(10), 1893–1903.
- Tarantola, A., 2005. *Inverse Problem Theory and Methods for Model Parameter Estimation*, Society for Industrial and Applied Mathematics.
- Tóth, Z., Spiess, V., Mogollón, J. M., & Jensen, J., 2014. Estimating the free gas content in Baltic Sea sediments using compressional wave velocity from marine seismic data, *Journal of Geophysical Research*, **119**, 1–17.
- Tóth, Z., Spiess, V., & Keil, H., 2015. Frequency dependence in seismoacoustic imaging of shallow free gas due to gas bubble resonance, *Journal of Geophysical Research*, **120**, 8056–8072.
- Vanneste, M., L'Heureux, J., Brendryen, J., Baeten, N., Larberg, J., Vardy, M., Steiner, A., Morgan, E., Forsberg, E., Kvalstad, C., Chand, T., et al., 2012. Assessing offshore geohazards: a multidisciplinary research initiative to understand shallow landslides and their dynamics in coastal and deepwater environments, Norway., *Advances in Natural and Technological Hazard Research*, **31**, 29–41.
- Vanneste, M., Longva, O., L'Heureux, J.-S., Vardy, M. E., Morgan, E., Forsberg, C., Kvalstad, T., Strout, J., Brendryen, J., Hafliðason, H., Lecomte, I., Steiner, A., Kopf, A., Morz, T., & Kreiter,

- S., 2013. Finneidfjord, a field laboratory for integrated submarine slope stability assessments and characterization of landslide-prone sediments: A review, in *Offshore Technology Conference held in Houston, Texas, USA - OTC 13OTC-P-686-OTC*.
- Vanneste, M., Forsberg, C., Knudsen, S., Kvalstad, T., L'Heureux, J., Lunne, T., Vardy, M. E., Chand, S., Longva, O., Morgan, E., Kopf, A., Morz, T., Steiner, A., Brendryen, J., & Haflidason, H., 2015. Integration of very-high-resolution seismic and cptu data from a coastal area affected by shallow landsliding - the Finneidfjord natural laboratory, *International Symposium on Frontiers in Offshore Geotechnics*, **3**.
- Vardy, M., 2015. Deriving shallow-water sediment properties using post-stack acoustic impedance inversion, *Near Surface Geophysics*, **13**, 143–154.
- Vardy, M., L'Heureux, J.-S., Vanneste, M., Longva, O., Steiner, A., Forsber, C., & j. Brendryen, 2012. Multidisciplinary investigation of a shallow near-shore landslide, Finneidfjord, Norway, *Near Surface Geophysics*, **10**, 267–277.
- Vardy, M., Vanneste, M., Henstock, T. J., Morgan, E., & Pinson, L., 2015. Can high-resolution marine geophysical data be inverted for soil properties?, *Proceedings of the Institute of Acoustics*.
- Vardy, M., Vanneste, M., Henstock, T. J., Clare, M. A., Forsberg, C., & Provenzano, G., 2017. State-of-the-art remote characterization of shallow marine sediments: the road to a fully integrated solution, *Near Surface Geophysics*, **15**, 387–402.
- Verbeek, N. & McGee, T. M., 1995. Characteristics of high-resolution marine reflection profiling sources, *Journal of Applied Geophysics*, **33**, 251–269.
- Virieux, J. & Operto, S., 2009. An overview of full-waveform inversion in exploration geophysics., *Geophysics*, **74**(6).
- Wilkins, R. & Richardson, M., 1998. The influence of gas bubbles on sediment acoustic properties: In situ, laboratory, and theoretical results from Eckernförde Bay, Baltic Sea, *Continental Shelf Research*, **18**, 1859–1892.